Check for updates

Water Resources Research

RESEARCH ARTICLE
10.1029/2021WR030584

Critical Zone Response Times and Water Age Relationships Under Variable Catchment Wetness States: Insights Using a Tracer-Aided Ecohydrological Model

Aaron A. Smith[1], **Doerthe Tetzlaff**[1,2,3], **Marco Maneta**[4,5], **and Chris Soulsby**[2,3]

[1]IGB Leibniz Institute of Freshwater Ecology and Inland Fisheries Berlin, Berlin, Germany, [2]Humboldt University Berlin, Berlin, Germany, [3]School of Geosciences, Northern Rivers Institute, University of Aberdeen, Aberdeen, UK, [4]Department of Geosciences, University of Montana, Missoula, MT, USA, [5]Department of Ecosystem and Conservation Sciences, University of Montana, Missoula, MT, USA

Abstract The dynamic relationships between water flux and storage, together with the associated water ages and speed of hydrological responses (as proxies for velocity and celerity respectively) are fundamental to understanding how catchments react to hydroclimate perturbations, such as floods and droughts. Using results from a calibrated, tracer-aided ecohydrological model (EcH_2O-iso) we analyzed the dynamics of storage-flux-age-response time (RT) interactions at scales that resolve the internal heterogeneity of these non-stationary relationships. EcH_2O-iso has previously shown an adequate representation of ecohydrological flux partitioning and storage dynamics (celerity), and water ages (velocity) over 11-year at Demnitzer Millcreek catchment (DMC, 66 km^2), a drought-sensitive, lowland catchment in Germany. The 11-year period had marked hydroclimatic contrasts facilitating the evaluation of flux-storage-age-RT dynamics under different wetness anomalies. Our results show that the spatio–temporal variability of soil moisture and ecohydrological partitioning dynamics reflect both land use (especially forest cover) and distinct soil units (i.e., brown earth vs. podzolic soils). Spatial differences in RTs of storage were driven by rapid soil evaporation and transpiration responses to rainfall, which revealed a divergence of transpiration ages from RTs. RTs of groundwater and streamflow were fast (days), but mediation by soil water storage dynamics caused marked separation from water ages (years-decades) of deeper flow paths. Analysis of RTs and ages revealed a degradation of process representation with coarsening model spatial resolution. This study uses novel analysis of the spatio-temporal interactions of flux-storage-age-RT from a model to understand the sensitivity and resilience of catchment functionality to hydroclimatic perturbations.

Key Points:

- Spatio-temporal variability of soil storage and ecohydrological partitioning was modulated by vegetation characteristics
- Transpiration, groundwater, and streamflow response times were distinct from water ages, with spatial differences driven by vegetation units
- Lower model resolution reduced spatial variability and increased the difference of catchment response and water age of fluxes and storages

Supporting Information:

Supporting Information may be found in the online version of this article.

Correspondence to:

A. A. Smith,
smith@igb-berlin.de

Citation:

Smith, A. A., Tetzlaff, D., Maneta, M., & Soulsby, C. (2022). Critical zone response times and water age relationships under variable catchment wetness states: Insights using a tracer-aided ecohydrological model. *Water Resources Research*, *58*, e2021WR030584. https://doi.org/10.1029/2021WR030584

Received 9 JUN 2021
Accepted 20 FEB 2022

Author Contributions:

Conceptualization: Aaron A. Smith, Chris Soulsby
Data curation: Aaron A. Smith
Formal analysis: Aaron A. Smith, Doerthe Tetzlaff, Marco Maneta, Chris Soulsby
Funding acquisition: Doerthe Tetzlaff
Investigation: Aaron A. Smith
Methodology: Aaron A. Smith, Marco Maneta
Project Administration: Doerthe Tetzlaff
Supervision: Doerthe Tetzlaff, Chris Soulsby

© 2022. The Authors.
This is an open access article under the terms of the Creative Commons Attribution License, which permits use, distribution and reproduction in any medium, provided the original work is properly cited.

1. Introduction

Analyses of the spatio-temporal dynamics of water fluxes, storage and associated ages in catchments are essential to understand how water resources respond to major perturbations in hydroclimatic drivers such as drought and floods (Dari et al., 2019; Guse et al., 2019; Köplin et al., 2012). Superimposed on these dynamic spatio-temporal interactions are the effects of long-term changes to land cover or induced by climatic variability (King & Karoly, 2017; Lorenz et al., 2019; Teuling et al., 2019) and differences in the frequency and intensity of hydroclimatic perturbations (Spinoni et al., 2017). Spatio-temporal variability of hydrological response to hydroclimatic drivers and perturbations is modulated by the physical and ecohydrological characteristics of catchments such as topography, geology, soil and vegetation cover (e.g., Shekhar et al., 2020); with the process-dominance of important interactions changing with scale (Fatichi et al., 2015). Identifying how these interactions vary within dominant catchment ecohydrological units provides an integrated understanding of complex process interactions and a segmentation strategy for evaluating hydrologic interconnections and responses at larger scales (Asbjornsen et al., 2011). This is important in the context of projected increases in air temperature and aridity, and changes in precipitation patterns, which may alter the reliability of water sources, reapportion the water balance and transform key ecohydrological couplings vis-à-vis between blue (soil water, groundwater, and streams) and green (evapotranspiration) water fluxes (Orth & Destouni, 2018), and in turn affect ecosystem stability (Ahmed et al., 2020; Marx et al., 2018; Okruszko et al., 2011).

Insights into the dynamics of complex ecohydrological couplings and connectivity between storage and fluxes in response to changing atmospheric conditions can be facilitated by an integrated understanding of celerity and velocity in hydrological systems, using response times and water ages as respective proxies (McDonnell &

Validation: Aaron A. Smith
Visualization: Aaron A. Smith
Writing – original draft: Aaron A. Smith
Writing – review & editing: Aaron A. Smith, Doerthe Tetzlaff, Marco Maneta, Chris Soulsby

Beven, 2014). While the use of measurement at a single location (e.g., discharge) or remotely sensed data (e.g., groundwater levels Van Loon et al., 2017) facilitates the evaluation of celerity at multiple scales by evaluating the propagation and dissipation of hydrologic responses, long-term in-situ measurements of tracers are indispensable in constraining estimates of water velocity. Tracers such as water stable isotopes have frequently been used to aid the estimation and interpretation of flow paths sustaining both blue and green fluxes (Dubbert & Werner, 2019; Sprenger et al., 2019) and the velocity of these flow paths through soil profiles, hillslopes, and catchments under varying wetness conditions (Ameli et al., 2016; Birkel et al., 2012; Harman, 2019; Pangle et al., 2017; Tetzlaff et al., 2014). However, the use of tracers has created two ways to interpret catchment function because tracer motion is controlled by particle velocity but fluxes and storages variations are controlled by celerity and hydraulic gradients (McDonnell & Beven, 2014). The differences between celerity and velocity responses result in the "old water paradox," where older, velocity-driven water is stored until a rapid event-driven release (Kirchner, 2003). The quantification of velocity and celerity aids in resolving the paradox; providing a deeper understanding of catchment non-stationarity (McDonnell & Beven, 2014) and their linkage to storage (Harman, 2019). Unfortunately, evaluations of both celerity and velocity in large hydrologic systems are uncommon, partially due to the limited number of large-scale catchments with long hydrometric and tracer records (Tetzlaff et al., 2017) which are required to constrain estimations and the limited number of analysis methods and models that couple water and tracer movement (Davies & Beven, 2015; van Verseveld et al., 2017).

Tracer-aided ecohydrological modelling helps to bridge the gap between plot-scale and watershed-scale measurements of water fluxes, storages, and water ages (Brewer et al., 2018; Soulsby et al., 2015). The development of such modelling integrates tracers, such as the water stable isotopes deuterium (^{2}H) and oxygen-18 (^{18}O), that can be used during model calibration and verification to improve and increase confidence in the spatio-temporal representation of water storage and flux dynamics for different soil and vegetation units (Guswa et al., 2020; Holmes et al., 2020; Kuppel et al., 2018; Smith et al., 2021). These models inherently estimate the speed of hydrologic response through the calibration and simulation of discharge, soil moisture, and groundwater dynamics. Tracer-aided approaches are also typically coupled with age-tracking (Danesh-Yazdi et al., 2018; Kuppel et al., 2020; Piovano et al., 2020), which provides an approximation of particle velocities in the model domain. Such models have been applied at multiple scales to quantify ecohydrological partitioning and evaluate water ages. However, interpretation of model results can be associated with large uncertainties of estimated velocities if tracer dynamics are damped, as well as the uncertainty of how model scale impacts the accuracy of partitioning (e.g., Smith et al., 2021; Surfleet et al., 2012).

The development of ecohydrological models that explicitly couple water partitioning in vegetation and soils, and also capture the scale dependence of these interactions (Fatichi et al., 2015), enables the evaluation of the effect of model scale on the estimated responsiveness of flux and storage dynamics. The sensitivity of water fluxes to vegetation dynamics underlines the importance of an appropriate representation of land cover heterogeneity in ecohydrological models. Further, there is process aggregation in model applications at coarse spatial and temporal resolutions that results in near-linear catchment response (Maneta et al., 2018) and low process resolution. Process aggregation in models often leads to a simplified, misleading representation of catchment behaviour. This process aggregation often leads to the "fallacy of the averages" (Wagner, 1969) in which multiple nonlinear processes are inaccurately averaged into a single linear response.

The main objective of this study was to improve understanding of the propagation of flow paths of both blue and green water at hydrologic meso-scales (~100 km^2), and how hydroclimatic perturbations affect internal spatio-temporal dynamics and aggregated catchment response and water demographics. The analysis of perturbations at subcatchment and aggregated scales facilitates the separation of the sensitivity of catchment internal flow velocities and response celerity to hydro-climatic anomalies. To achieve this overarching objective we used data-driven modelling results from the Demntizer Millcreek catchment (DMC) mesoscale catchment in Germany to answer the following specific research questions:

1. What are the roles of blue and green water fluxes and catchment storage dynamics in modulating both short-term and seasonal hydroclimatic perturbations?
2. What are the associated spatio-temporal dynamics, and are there distinct dissociations of hydrologic response times and water ages for the major water stores and fluxes in the catchment?
3. What is the influence of model resolution on the identifiability and characteristics of simulated spatio-temporal patterns of storage-flux-age-response time (RT) dynamics?

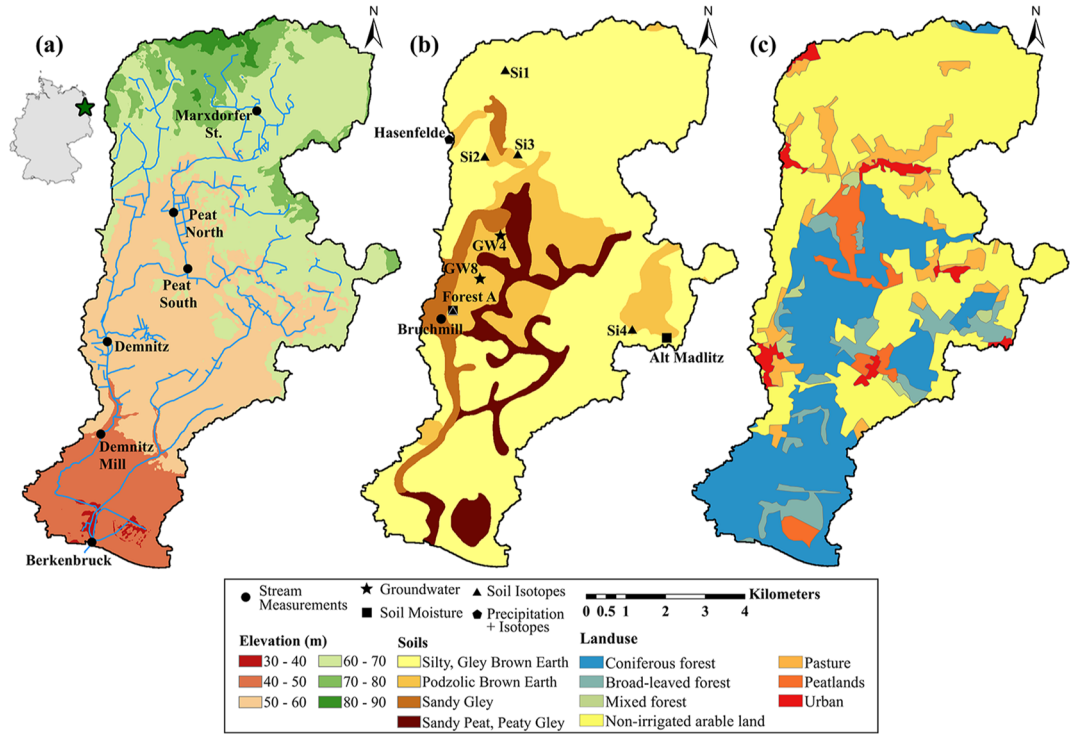

Figure 1. Demnitzer Millcreek catchment (a) topography, (b) dominant surficial soils, and (c) primary land use (Landesamt für Umwelt (LfU, 2019)). Channels and stream measurement locations are shown on the topography map; soil and groundwater measurements are shown on the soil map.

2. Study Site and Methods

2.1. Study Site

The Demnitzer Millcreek (DMC) is a mesoscale catchment (66 km^2) situated in northeast Germany, 50 km southeast of Berlin (Figure 1a). It is located in the central North European Plain which contains major rivers (e.g., Rhine, Oder, and Elbe), large cities needing substantial drinking water supplies, and is an important agricultural region (Gutzler et al., 2015). The DMC is a mixed land use catchment dominated by agriculture in the North and forests in the South (Figure 1c) and has been used as a long-term (>30 years) monitoring site for hydrology and biogeochemistry (Gelbrecht et al., 1996, 2005; Smith, Tetzlaff, Gelbrecht, et al., 2020). The catchment has undergone significant changes since the early 1990s due to changing management practices with stream naturalization, removal of tile drainage, and wetland restoration in the mid-reaches of catchment between locations Peat North and Peat South (Figure 1a) (Smith, Tetzlaff, Gelbrecht, et al., 2020).

2.1.1. Soils and Vegetation

The geology of the DMC is predominantly glacial-fluvial deposits through the mid- and south areas of the catchment and base moraine in the North, which were deposited during the Pleistocene glaciation (Gelbrecht et al., 2005). The catchment contains four relatively freely draining soil units: silty brown earth (72%), podzols (14%), sandy gleys (5%), and peaty gleys (9%; Figure 1b). The silty brown earth dominates the North area with podzolic soils surrounding the peaty gleys in the wetlands and sandy gleys fringing channels in the South. Vegetation closely reflects the dominant soils and is characterised by four primary units: arable agricultural lands (52%), coniferous forests (29%), pasturelands (13%), and broadleaf forests (6%; Figure 1c). Agricultural lands in the headwaters of the DMC undergo annual rotations with maize, winter wheat, and barley (Kleine et al., 2020; Smith, Tetzlaff, Gelbrecht, et al., 2020). Plantations of Scots pine (*Pinus sylvestris*) and additional coniferous forests dominate vegetation in the South and mid-reaches of the catchment. Poor soil quality in the wetlands coupled, with the naturalisation of land management practices (i.e., no draining), inhibits arable crops and results in the use of wetlands as short grass-dominated pasturelands for livestock grazing. Broadleaf forest dominated by

Table 1
Average Annual Atmospheric Conditions in the Demnitzer Millcreek Catchment From 2009 to 2019

Year	Precipitation (mm)	Relative humidity (%)	Air temperature (°C)
2009	605.5	78.6	9.4
2010	775.9	79.3	8.1
2011	611.7	76.4	10.0
2012	587.0	77.7	9.4
2013	580.0	79.2	9.3
2014	497.9	79.4	10.7
2015	481.8	75.2	10.5
2016	504.4	77.1	10.0
2017	665.7	78.5	10.0
2018	382.8	72.9	10.9
2019	495.2	73.9	11.1
Average	575	77.1	10.0

Note. Wind speed not shown as it does not show interannual changes (3.1 m/s).

birch (*Betula pendula*), European beech (*Fagus sylvatica*), and oak (*Quercus robur*) covers remaining small areas (Kleine et al., 2020).

2.1.2. Climate

The climate of DMC is continental with a maritime influence (Köppen Index). The DMC has relatively low precipitation and high radiation, resulting in high evapotranspiration (ET; ∼90% of precipitation; Smith et al. (2020b)). Precipitation has larger inter-annual variability, with amounts in wet years being double than drought years (382–776 mm; Table 1). Since 2009, there has been a modest, but significant decrease in precipitation of ∼20 mm/year (p-value < 0.01). Average winter temperatures are +0.5°C in January (2007–2020; DWD (2021)). Converse to precipitation, the annual air temperature has moderately increased by 0.2°C/year since 2009 (Table 1) (p-value < 0.01).

Coupled with precipitation and temperature, relative humidity is low in warm, drier summers (66%; 2007–2020) and high in cold, wet winters (88%; 2007–2020). The growing season (May–September) has high variability of daily average humidity, ranging from 40% to 100% (skewness = 0.01). Winters (November–February) exhibit low variability (70%–100%; 5th–95th percentile) with a high skew to saturated air (skewness = −0.83). Similar to precipitation, relative humidity has progressively decreased since 2009 (p-value < 0.01) by 0.4%/year (Table 1).

2.1.3. Hydrologic and Isotope Data Collection

Climate data at weather stations surrounding the catchment were collected by Deutscher Wetterdienst weather stations (DWD, 2021) throughout the study period (Table 2). An additional automatic weather station (AWS, Environmental Measurement Limited, UK), located in the North West of the catchment was installed in 2018 (Figure 1). Gridded short and long-wave radiation data over the catchment were extracted from ERA5 reanalysis products (ECMWF, 2021), which has been previously used for the region (Douinot et al., 2019).

Table 2
Measurements of Forcing, Hydrological, and Isotopic Data (δ^2H and $\delta^{18}O$) in the Demnitzer Millcreek Catchment

Measurement type	Locations	Resolution	
		Spatial	Temporal
Forcing datasets			
Meteorological data	Lindenberg, Manschnow, Neu Madlitz, Muncheberg, Furstenwalde	n/a/	Daily
Short & longwave radiation (W/m^2)	n/a/	500 m	Daily
Precipitation isotopes	Hasenfelde	n/a	Daily
Leaf Area Index (m^2/m^2)	n/a/	500 m	8-day average
Calibration and validation datasets			
Soil moisture	Forest A, Alt Madlitz	n/a	Daily
Bulk soil isotopes	Forest A, Si1, Si2, Si3, Si4	n/a	Monthly
Groundwater isotopes	GW4, GW8	n/a	Monthly
Sap flow (L/day)	Forest A	n/a	Daily
Evapotranspiration (mm/day)	n/a	500 m	8-day average
Discharge (m^3/s)	Demnitz Mill, Demnitz	n/a	Daily
Discharge isotopes	Peat North, Peat South, Demnitz Mill	n/a	Weekly
	Bruchmill	n/a/	Daily

Note. Meteorological data encompasses precipitation, wind speed, humidity, and temperature. n/a/indicates not applicable.

Soil moisture has been measured at 20, 60, and 100 cm depths since 2018 in a forest and grassland in the West (Forest A; Figure 1b) (Kleine et al., 2020). A third soil moisture measurement location was installed in 2019 in an agricultural area in the East (Alt Madlitz; Figure 1b) (Smith et al., 2021). Daily groundwater levels have been measured in the mid-reaches and stream water discharge in the south of the catchment since 2001 (Smith et al., 2021). Sap flow was measured in a mixed forest stand at Forest A in 2018 (Figure 1b). Composite 8-day evapotranspiration and latent heat estimates were extracted from the MODIS MOD16A2v006 product at 500 m resolutions (Running et al., 2017).

Collection of water stable isotopes samples for deuterium (δ^2H) and oxygen-18 ($\delta^{18}O$) analysis began in 2018 as event-based precipitation sampling from the AWS, biweekly sampling from streams at seven sites, monthly groundwater samples, and monthly bulk soil samples from multiple depths (Figures 1a and 1b, and Table 2) (Kleine et al., 2020; Smith et al., 2021). The autosampler bottles contained a layer of paraffin to prevent evaporation. Bulk soil samples were collected and immediately placed in sealed bags and analyzed using the direct equilibrium method (details in Kleine et al. (2020)). δ^2H and $\delta^{18}O$ were analysed with a Picarro L2130-I cavity ring-down analyser (Picarro, Inc., Santa Clara, CA, USA) with a precision of 0.5‰ for δ^2H and 0.1‰ for $\delta^{18}O$. Samples were examined for organic contaminants using the Chem-Correct Software (Picarro, Inc.), and contaminated samples were discarded.

2.1.4. Hydrology of the Demnitzer Millcreek Catchment

The hydrology is dominated by green water fluxes, with limited groundwater recharge (~16% of precipitation) mainly occurring in winter (Smith, Tetzlaff, Kleine, et al., 2020; Smith et al., 2021). Deeper groundwater is linked to a regional groundwater system; however, there is limited connectivity of regional groundwater to surface water in DMC except for near the outlet (Smith, Tetzlaff, Gelbrecht, et al., 2020). Low intensity, high-frequency winter precipitation events coupled with low ET replenish catchment storage while high summer ET decreases catchment storage and results in frequent cessation of streamflow despite intermittent high-intensity convective summer storms (Kleine et al., 2021). Spatial patterns of ecohydrological fluxes are controlled by differences between soil-vegetation units. Lower ET and shallower rooting depths in the agricultural areas result in a majority of runoff generation from the agricultural areas in the North where there is more consistent annual groundwater recharge (Smith et al., 2021). Rapid runoff generation in the North is facilitated by historical channel enlargement and increased drainage which also connected natural glacially-formed wetlands (Gelbrecht et al., 2005). Wetlands in the mid-reach and near the outlet of the catchment are hotspots for evaporation due to consistent high wetness relative to the rest of the catchment and are important saturated areas for runoff generation (Smith, Tetzlaff, Gelbrecht, et al., 2020; Smith et al., 2021). The previous restoration of wetlands in the mid-reach of the catchment (2000–2001) helps to attenuate flow response due to a combination of the restoration and beaver dams (Smith, Tetzlaff, Gelbrecht, et al., 2020). Water ages throughout the catchment have previously been shown to be relatively old (Smith et al., 2021) with spatial patterns that are dependent on vegetation and soil units. Water ages in deeper soils and groundwater are decadal with younger water in upper soils (months) and discharge (years; cf. Kleine et al. (2021)).

2.2. EcH$_2$O-Iso: Tracer-Aided Ecohydrological Modelling

EcH$_2$O-iso is a physically-based, tracer-aided distributed ecohydrological model. It is based on an integrated approach to solving canopy, surface, and soil energy and water balances, with a dynamic vegetation conceptualisation and a tracer module that tracks δ^2H, $\delta^{18}O$, and water age (Kuppel et al., 2018; Maneta & Silverman, 2013). The model has previously been calibrated against multi-criteria data (see Section 2.2.3) in DMC at four model resolutions ranging in 250–1,000 m square grids (for full details see Smith et al. (2021)). A brief overview of the model is in the following sections and a conceptual diagram of the model structure is in the Supplementary Material to aid interpretation of model results (Figure S1 in Supporting Information S1). Original descriptions of the model are presented in Maneta and Silverman (2013) and Kuppel et al. (2018).

2.2.1. EcH$_2$O-Iso Energy Balance

The energy balance is estimated using a top-down approach with data on incoming short-and long-wave radiation rates, air temperature, wind speed and air relative humidity to estimate the canopy and surface net radiation, canopy and surface temperature, and latent, and sensible heat exchanges between soil and canopy and the atmosphere. Latent heat exchanges associated with transpiration and evaporation of water intercepted by the canopy,

and from soil evaporation are differentiated in the model. Latent heat of transpiration is limited by leaf stomatal and aerodynamic resistances, atmospheric vapour pressure deficits, and soil water availability. Latent heat of evaporation from the soil and the canopies is controlled by water availability in the topsoil and on the surface of leaves, by atmospheric aerodynamic resistances and in the case of soils, also by soil resistance to gas exchange. Canopies alter the surface energy balance by reducing the fraction of shortwave radiation incident to the surface (shading), by increasing the atmospheric aerodynamic resistance to latent and sensible heat exchanges between the atmosphere and the soil surface, and by emitting longwave radiation downward onto the soil. The components of the surface energy balance track the dynamics of ground heat to calculate soil temperatures in two thermal layers as a function of latent heat and sensible heat exchanges, heat conduction within the soil, and net radiation relationships. Ground heat storage is dependent on soil thermal properties (thermal capacity and conductivity) which are dependent on soil moisture contents. Surface latent heat exchanges are influenced by the aerodynamic and soil resistance to evaporation.

2.2.2. EcH$_2$O-Iso Water Balance and Tracer Mixing

Similar to energy, the water balance is estimated top-down from the canopy to the surface, to the sub-surface. Precipitation enters the canopy and is either intercepted (capacity permitting), or translocates and reaches the surface as throughfall. Intercepted water leaves the canopy only through canopy evaporation. At the surface, ponded water from throughfall infiltrates using the Green-Ampt model, and gravity drainage is used to vertically redistribute water when moisture exceeds field capacity. Upward water movement can occur from deeper soils when they are fully saturated. Soil evaporation is estimated from the first soil hydrologic layer using latent heat obtained from the energy balance. Groundwater is laterally routed using a kinematic wave model with momentum linearly proportional to the local cell slope. Ponded water on the surface at the end of the time-step is routed to the next downstream cell, or to the channel (if present within the cell) as overland flow allowing for reinfiltration along the flow path. Channel routing is conducted using a nonlinear kinematic wave model. Mixing of water ages in each storage (i.e., layers 1–3) is estimated using the complete mixing assumption, where incoming water is completely mixed with water in storage. Incoming water (precipitation) is assigned an age of 0 days. The water age of fluxes is the flux weighted average of the water age of each source storage. At the end of each time-step, the water age in storage is incrementally increased by one time-step.

2.2.3. Model Setup, Parameterization and Calibration

Previous calibration of EcH$_2$O-iso in the DMC (Smith et al., 2021) formed the basis for the novel analysis of modeled outputs conducted in this study. A brief description of the modelling process follows with further details of model calibration, validation, and evaluation presented in the original paper. The DMC was set up for daily time-steps in EcH$_2$O-iso at four spatial resolutions; 250, 500, 750, and 1,000 m square cells. The proportions of soil and vegetation units per cell area were aggregated for the corresponding cell size prior to each model run. Model forcing data (precipitation, wind speed, relative humidity, and air temperature) were taken from surrounding Deutscher Wetterdienst stations (DWD, 2021). Forcing data was applied within the catchment using the distance to the surrounding measurement locations. Morris sensitivity analysis (Morris, 1991; Soheir et al., 2014) was conducted to optimize the number of calibrated parameters using radial sampling with 75 trajectories. The most sensitive parameters for soil, vegetation, and channels identified by the average of the trajectories were used in calibration (Table 3).

Latin hypercube sampling was used to generate 100,000 parameter sets for Monte Carlo simulations. Multi-criteria calibration (Table 2) was used to constrain parameters on model configurations of fluxes and storages of water and energy for each spatial resolution (Smith et al., 2021). Multi-criteria calibration was conducted independently for each model resolution. For subsequent analysis, the 100 "best" behavioural simulations identified by the multi-criteria calibration for each model configuration were retained from the 100,000 parameter sets. Modelled fluxes and storages for each model resolution were generally within 10%–15%, with larger uncertainties in water ages, increasing with model resolution.

Table 3
Model Parameters for Soil, Vegetation, and Channel Used in the Calibration of EcH2O-Iso

Soil parameters	Vegetation parameters
Horizontal hydraulic conductivity (m/s)	Maximum stomatal conductance (m/s)
Porosity (m^3/m^3)	Light sensitivity for conductivity (-)
Air entry pressure (m)	Vapour pressure deficit sensitivity for conductivity (-)
Brooks-Corey parameter (-)	
Soil depth (m)	Maximum canopy storage (m/LAI)
Vertical soil anisotropy (-)	Beer's law light aattenuation coefficient (-)
Channel seepage parameter (-)	Exponential root distribution parameter (1/m)
Soil Albedo (-)	Channel properties
Snow melt coefficient (m/sC)	Manning's n roughness ($s/m^{1/3}$)
Bedrock Leakance parameter (-)	Channel surface roughness (-)

2.3. Spatiotemporal Analyses

2.3.1. Standardized Indices

Standardized indices like the standardized precipitation index, (SPI; McKee et al. (1993)), are used to quantify anomalies in the time series of hydrologic variables such as fluxes and storages by transforming the original variable into standard normal deviates with respect to the long-term average. Deviations with respect to the mean can be accumulated over different periods using a moving window to produce the time series of anomalies at different time scales (e.g., time series of anomalies accumulated over a 6-month time scale). Standardized index time scales of 3 months or shorter capture the effects of higher-frequency anomalous events, while time scales 6 months or longer can represent the effect of long term anomalies generated by processes with longer characteristic time scales (McKee et al., 1993). The standardized index for precipitation, relative humidity, air temperature, and wind speed (P, RH, T_a, and w, respectively) was calculated for each variable using the Standardized Precipitation Index MATLAB package (Lee, 2021). Long-term climatic trends were not removed as changes were not large and would dampen the influence of extreme events. The package utilizes gamma distribution fit parameters α and β the raw data were used to estimate the cumulative gamma distribution:

$$F(x(ts)) = (1 - n) + n * \frac{1}{\Gamma(\alpha)} * \gamma(\alpha, \beta * x(ts)) \quad (1)$$

where Γ is the gamma function, γ is the lower incomplete gamma function, $x(ts)$ is the moving average raw data with time scale ts, and n is the fraction of data that are non-zero. The cumulative gamma distribution was then transformed to the inverse normal distribution:

$$T_{inv}(x(ts)) = -\sqrt{2} * \text{erfc}^{-1}(2 * F(x(ts))) \quad (2)$$

Using the same procedure described above, we estimated standardized indices in each model cell (2009–2019) for deseasonalized soil moisture storage in soil layers 1, 2, and 3, transpiration, evaporation, groundwater flow, and discharge fluxes. Analysis of transpiration anomalies was restricted to the growing season. As with the climatic indices, long-term trends in storage and fluxes were maintained to better evaluate large events. All standardized indices were calculated at three time scales (30-, 90-, and 180-day).

2.3.2. Spatial Analysis

The relative importance of P, RH, T_a, w, and SM anomalies on transpiration dynamics was evaluated for each model pixel and model spatial resolution using multi-variate regression of the standardized indices (95% confidence limits). Since the climatic inputs and transpiration variables are standardized, if the inputs are uncorrelated the multiple regression coefficients yield the partial relative importance of each variable in explaining transpiration anomalies (Wurster et al., 2020). The coefficients were normalized to sum to 1 for each model cell to provide inter-cell and scale comparability.

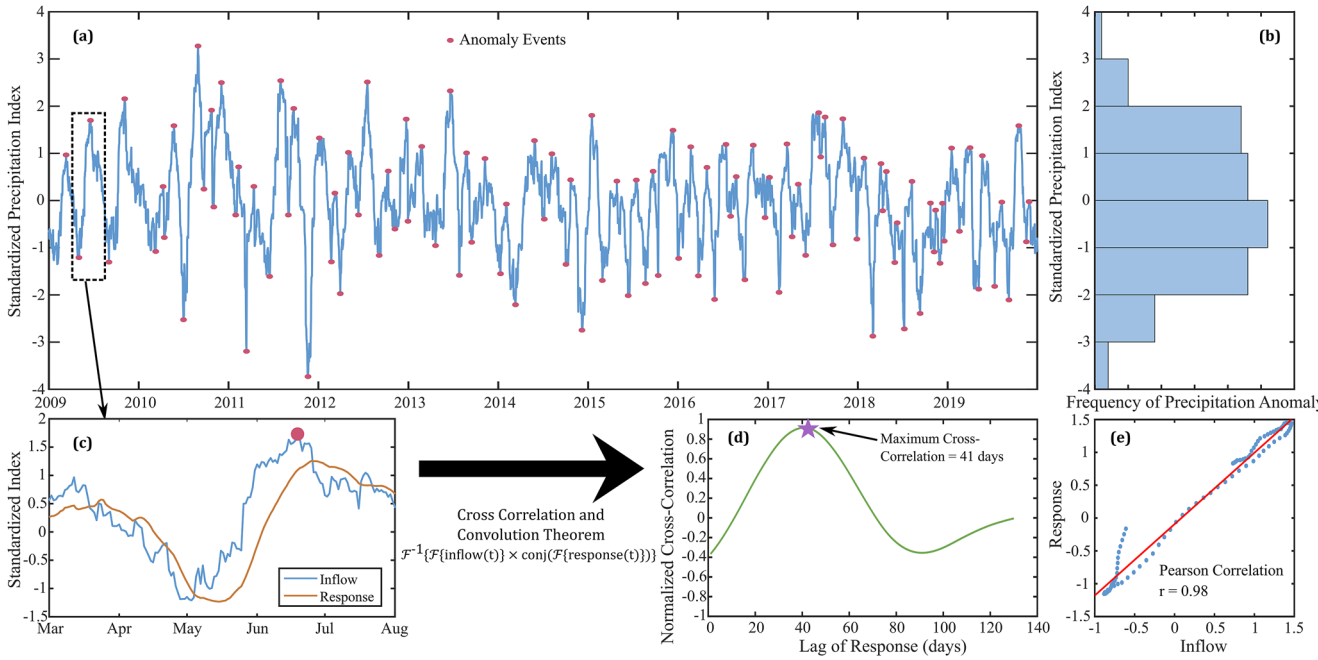

Figure 2. Summary of methodological steps to assess coherence in temporal variability: (a) Example standardized precipitation index (SPI) used as input flux, with red circles indicating a maximum/minimum anomaly event. The dashed box indicates a specific event shown in (c). (b) Histogram of the number of anomaly events of the example SPI. (c) Example inflow and response standardized indices for the anomaly event in the black square in (a). (d) Cross-correlation of inflow and response for different response times. (e) Pearson correlation of inflow and response at the optimal max cross-correlation.

The evaluation of storage and flux sensitivity to variations in catchment wetness can identify the roles of blue and green water in modulating the susceptibility catchment water availability to hydroclimatic variability. For each model cell and all resolutions, the variation was evaluated as the change in the average range of soil moisture or fluxes (non-standardized) between the wettest ($1.5 < \text{SPI} < 2$) and driest ($-2 < \text{SPI} < -1.5$) precipitation anomalies. The range of fluxes or storages from wet to dry were evaluated only for summer months (May–September) and SPI anomalies representing inter-annual differences in catchment wetness as transpiration and soil evaporation were only dominant during the growing season.

We conducted stepwise multi-variate regression of water ages and RT to spatial features to evaluate the spatial heterogeneity of water fluxes within the catchment. Spatial features include the percentage of vegetation units, soil units, and slope, which were all previously shown to have an independent high correlation with estimated water ages (Smith et al., 2021). The significance of each variable to explain spatial changes in water age and RT was evaluated using regression analysis. The analysis was conducted at the 95th confidence limit (p-values < 0.05). The relative importance of each significant variable was evaluated by the proportionate increase of R^2 of the multi-variate regression fit.

2.3.3. Temporal Variability of Water Ages and Response Times

The time difference (i.e., RT) between hydroclimatic perturbations and the resulting spatio-temporal dynamics of fluxes and storages within the catchment were estimated using the respective standardized indices (Figure 2a). The variability of RTs and water ages are additionally influenced by the temporal dynamics of different wetness conditions (e.g., Botter et al., 2010; Davies & Beven, 2015; Rinaldo et al., 2011) as well as the time scale of the standardization. Therefore time scales of 30-, 90-, and 180-day were used to identify the response of the catchment storage and fluxes to short, intermediate and seasonal wetness conditions. Due to the implications of changes in transport rates (i.e., water age and contaminant velocity, Kirchner et al., 2000) and flow propagation as well as water availability (e.g., Orth & Destouni, 2018) we further evaluated the water ages and RTs at different wetness states.

To isolate the catchment response to different precipitation anomalies (i.e., anomaly not as part of a larger anomaly), we identified independent anomaly events for each time scale by the prominence of the anomaly peak or

trough, defined by the intrinsic height of the anomaly relative to the surrounding events (example in black box in Figure 2a). The prominence threshold was optimized to maximize the total number of events with an additional goal of a uniform distribution of event occurrence between SPI anomalies of −2 and 2 (Figure 2b).

In this study, we evaluated the RT as the time-elapsed for the maximum cross-correlation of the event inflow anomaly signal (e.g., SPI) to the anomaly response (e.g., standardized soil index) of a hydrologic compartment (as a proxy for the celerity; Figures 2c and 2d). Thereby the RT may differ from the time-elapsed between the peaks of inflow to response signals. The use of the elapsed time provides a relative measure of the response to input which is inter-and intra-annually comparable. The cross-correlation was estimated using the convolution theorem, where input and response time-series are translated into the frequency domain using fast Fourier transforms (Box et al., 1994; Frigo & Johnson, 1998). The cross-correlation (C) is estimated as:

$$C = \mathcal{F}^{-1}(\mathcal{F}(inflow) \times conj(\mathcal{F}(response))) \quad (3)$$

where $\mathcal{F}$ is the Fourier transform and *conj* is the complex conjugate (translation of Figures 2c and 2d). The strength of RT was evaluated using correlation coefficients (Figure 2e). Cross-correlation analysis was conducted for each input event (i.e., Figure 2a), time scale (30, 90, and 180-day), and model cell of each resolution (250, 500, 750, and 1,000 m). The RT of modelled soil layers 2 and 3 were estimated using the modelled standardised index of the layer above as the input signal (layers 1 and 2, respectively).

The relationships of water age and RT to SPI were used to understand the variability of catchment response at different anomalies and evaluated using least-square regression. The strength of the relationships was evaluated to a 95% significance level.

3. Results

3.1. Variability of Atmospheric Drivers

Hydroclimate in DMC has been highly variable since 2009 (Table 1), with the SPI varying from extreme wet conditions in 2010 and 2011 (SPI > 2) to extremely dry conditions during the drought of 2018 ($-2 < \text{SPI} < -1.5$; Figure 3a). Short time scale anomalies in SPI (30-day) were—unsurprisingly—the most variable during the wettest and driest extremes. The longer time scale SPIs (90 and 180-day) had more persistent anomaly periods throughout the study (Table S1 in Supporting Information S1). The phase of the SPI had a dependency on the time scale and shifted ∼0.47 days per time-scale day (not shown). The longer time-scale SPI showed a gradual long-term drying trend leading from the sustained wet conditions at the beginning of the study period to dry conditions toward the latter years. The drying during the study period (2009–2019) was more exaggerated than long-term change over the standardization record (30-year, 1990–2020).

The standardized temperature index (STI), standardized relative humidity index (SRHI), and standardized wind index (SWI) showed more muted dynamics compared to the SPI, but also clear trends (Figures 3b–3d). The drier years (2018–2019) showed notable changes in both the STI and SRHI, with higher temperatures and lower humidity (Figures 3b and 3c). The SRHI only showed sustained anomalies during periods of low precipitation (e.g., post-2011 and mid-to-late 2018), with a low average duration (Table S1 in Supporting Information S1). The SWI did not show any collinearity with SPI, STI, or SRHI, with only periodic overlaps (e.g., summer 2011, Figure 3d). Catchment outflow and groundwater level (as a proxy of groundwater storage; Figures 3e and 3f) were strongly related to SPI, with the highest discharge and groundwater levels at the beginning of the study period, decreasing throughout the study.

3.2. Sensitivity of Storages and Blue and Green Water Fluxes to Variations in Catchment Wetness

The transition of soil moisture from dry to wet conditions was largest in the upper soils in the main agricultural areas and in agricultural land fringing the wetlands in the mid-catchment (Figures 4a and 4b). Conversely, wetlands and conifer forests dominate areas with damped soil water content response in the upper soils (Figures 4a and 4b). The large transformation of soil moisture in deeper soils revealed a large influence of conifer cover from dry to wet conditions (Figures 4c–4f).

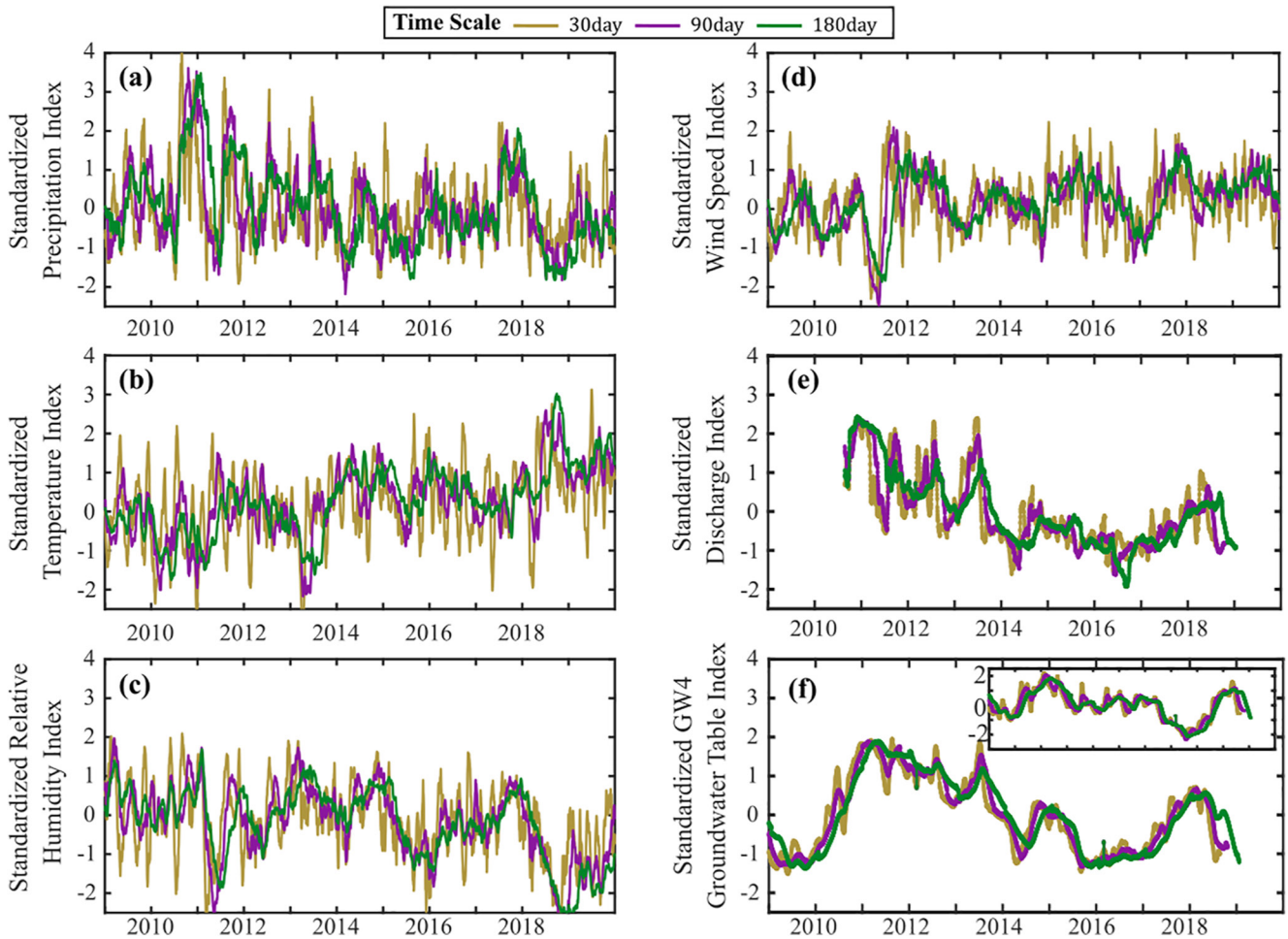

Figure 3. (a) Standardized precipitation index, (b) standardized temperature, (c) standardized relative humidity, (d) standardized wind speed, (e) standardized discharge at Demnitz Mill, and (f) standardized groundwater table in GW4 (GW8 in subplot) of 30, 90, and 180-day time scales.

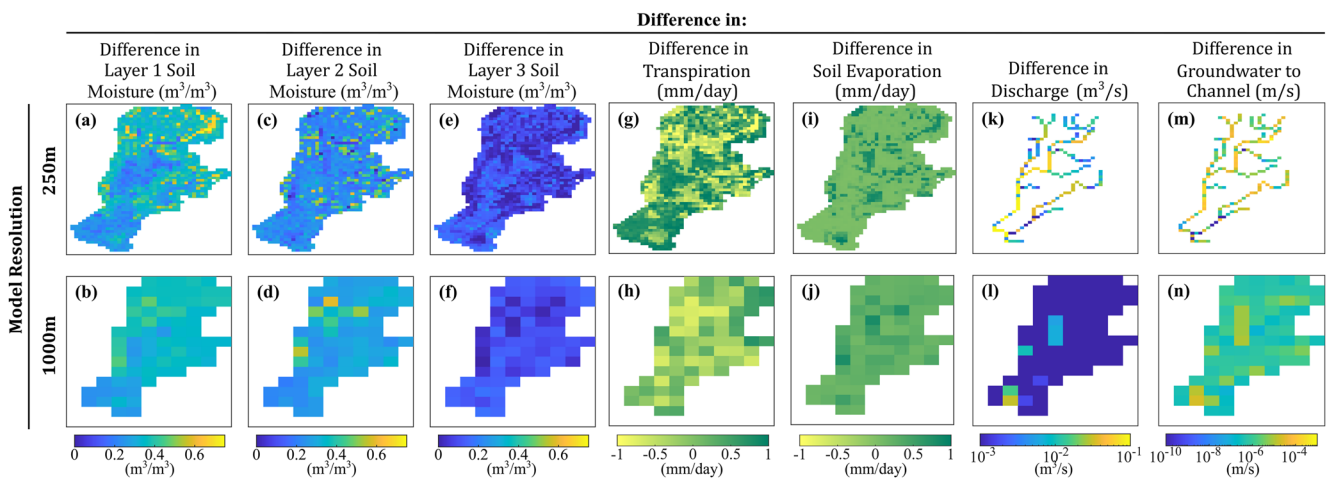

Figure 4. Differences in the summer months for the average dry (SPI < −1.5) to wet (SPI > 1.5) storage (a–f) and fluxes (g–n) across the catchment for 250 and 1,000 m model resolutions (all resolutions in Figure S3 in Supporting Information S1). Positive values indicate an increase in average storage or flux from dry to wet periods.

The correlation between transpiration flux and wetness was limited compared to soil moisture (Figure S2 in Supporting Information S1). Maximum transpiration occurred during average conditions (SPI = 0) and was lower under extreme wetness anomalies due to lower atmospheric water demand and water availability (Figure S2 in Supporting Information S1 and Section 3.3). In the conifer and agricultural areas, a general increase in catchment wetness produced higher transpiration (Figures 4g and 4h); while atmospheric conditions and vegetation properties in the pasturelands lowered the difference of transpiration from dry to wet conditions (Section 3.3).

Soil evaporation, discharge, and groundwater flow all had large transitions from dry to wet conditions, with discharge and groundwater flow increasing nonlinearly with increasing wetness (Figures 4i–4n, and Figure S2 in Supporting Information S1). Higher wetness stimulated higher discharge and groundwater flow particularly in the wetlands and conifer forests (Figures 4k–4n).

Model resolution affected the spatio-temporal variability in the range of storage and fluxes of blue and green water to variations in catchment wetness (Figure 4 and Figure S3 in Supporting Information S1 for all model resolutions). Spatial variability of the shallow soil moisture transition from dry to wet was relatively consistent across model resolutions, with aggregation in upscaling showing reduced extreme values. Intensified aggregation of soil moisture in deeper soils resulted in larger spatio-temporal differences between model resolutions, most notably in the eastern agricultural areas (Figures 4e and 4f).

The spatio-temporal relationships of transpiration flux with system wetness showed the largest differences between model resolutions. At coarse model resolutions (750 and 1,000 m), atmospheric conditions and vegetation properties caused limited spatial variability and a negligible increase in simulated transpiration between wet and dry conditions (Figure 4h and Figure S3 in Supporting Information S1). The nonlinear increase and spatial variability with wetness were much less apparent for discharge and groundwater flow at coarser model resolutions (Figures 4l and 4n, and Figures S2–S3 in Supporting Information S1).

3.3. Spatio-Temporal Variations in Atmospheric and Soil Moisture Controls on Transpiration

Transpiration was controlled by both supply and demand of vapour pressure deficit (VPD) and soil moisture, and aerodynamic and stomatal resistances (Section 2.2.1, EcH_2O-iso model structure). Transpiration rates can be limited even when soil moisture is available due to low wind speed or VPD. Therefore correlations of transpiration anomaly to precipitation anomaly are mediated by other hydroclimatic perturbations that exert varying control at different time-scales (Figure S2 in Supporting Information S1). The influence of the soil moisture, precipitation, humidity, wind speed, and air temperature anomalies in explaining transpiration anomalies was analyzed across the catchment using multi-variate regression with each time scale. Within this section (3.3) the terms precipitation, soil moisture, humidity, wind speed, air temperature, and transpiration refer to their respective anomalies.

There was large spatial variability in the importance of factors regulating transpiration, which mostly followed land use patterns (Figure 5, though also see all model resolutions of 30, 90 and 180-day time scales on Figures S4–S6 in Supporting Information S1). Soil moisture was of greatest importance in governing conifer transpiration (Figures 5a and 5b), which corresponded to the largest change of transpiration rates from dry to wet (Figures 4g and 4h). Humidity had stronger control on transpiration in the agricultural areas and wetlands (Figures 5e and 5f). High and low wetness conditions, corresponding to low VPD and low stomatal conductance with high VPD, respectively, most strongly controlled transpiration in the agricultural areas and wetlands in the north and mid-reaches of the catchment.

Controls of precipitation, wind speed, and air temperature on transpiration were spatially consistent. Of these three, air temperature showed the strongest influence on transpiration at short time scales (30-day, Figures 5i and 5j). Seasonal time scales (180-day) revealed an increased influence of precipitation on transpiration in the conifer forests and a decreased control of humidity on transpiration in the agricultural areas (Figure S6 in Supporting Information S1).

Model resolution also influenced the spatial identification of controls on transpiration, similar to the effect of resolution on storage and flux variability (Figure 4). In particular, the control of soil moisture on transpiration in the conifer forests was less apparent at coarser resolutions (Figures 5b, 1,000 m), revealing an averaging to a higher control of relative humidity on transpiration (Figure 5f).

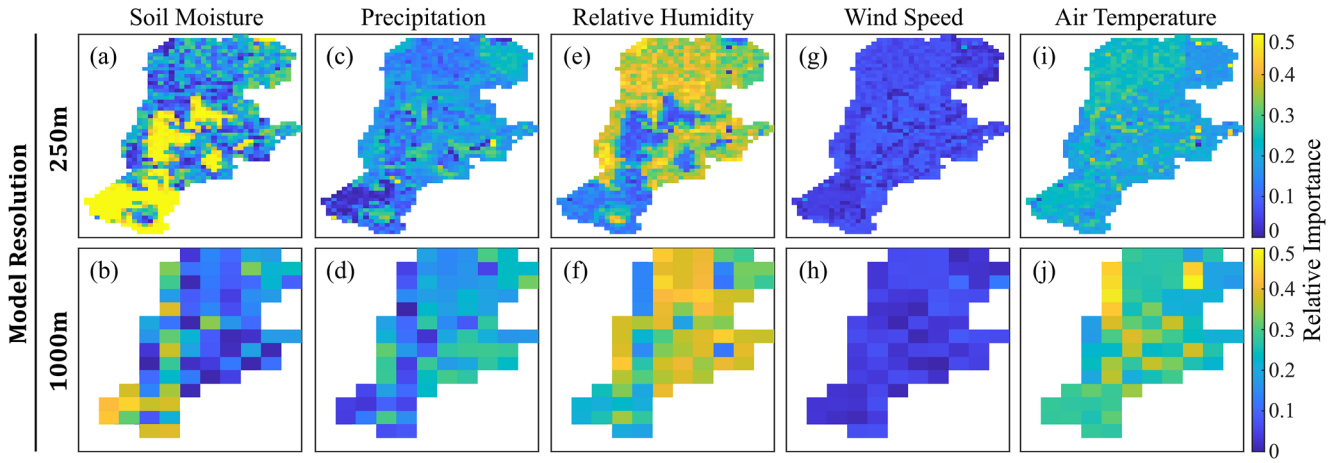

Figure 5. Controls of soil moisture, precipitation, relative humidity, wind speed and temperature anomalies on transpiration anomalies for the 30-day time scale. Colour maps indicate the relative importance (sum to 1 for each model cell) of each variable on controlling total summer transpiration (all resolutions for 30, 90, and 180-day time scales in Figures S4–S6 in Supporting Information S1).

3.4. Response Times of Storages and Fluxes of Blue and Green Water to Hydroclimatic Perturbations

Spatial patterns of the RT for all time-scales (30, 90, and 180 days) were very similar; therefore, the RTs averaged for all time scales are shown for ease of spatial interpretation and are not shown for each time-scale. Shallow soil layers in the northern agricultural areas exhibited the shortest RTs (Figures 6a and 6b). Additionally, correlation coefficients were highest in the upper soils (*r*-values; Figure S7 in Supporting Information S1). Considerably longer RTs characterised the lower soils, with a much longer RT in the southern conifers than in the northern agricultural areas (Figures 6a and 6b). The RTs of transpiration were exponentially longer in areas with a higher proportion of agricultural lands (Figures 6g and 6h). The faster RT of the conifer land cover aligned with the areas where soil moisture anomalies had the strongest controls on transpiration anomalies (Figures 5a and 5b). The average RT of soil evaporation to soil moisture was very short, with areas of higher pasturelands proportions showing longer RTs (Figures 6i and 6j). Similar to the RTs of soil moisture to precipitation anomalies, the RTs of groundwater flow and discharge anomalies to precipitation anomalies were the shortest in the agricultural areas (Figures 6k–6n). The RTs of groundwater flow to precipitation anomalies were exponentially longer in areas with higher conifer forests proportions than in areas of greater agricultural areas proportions.

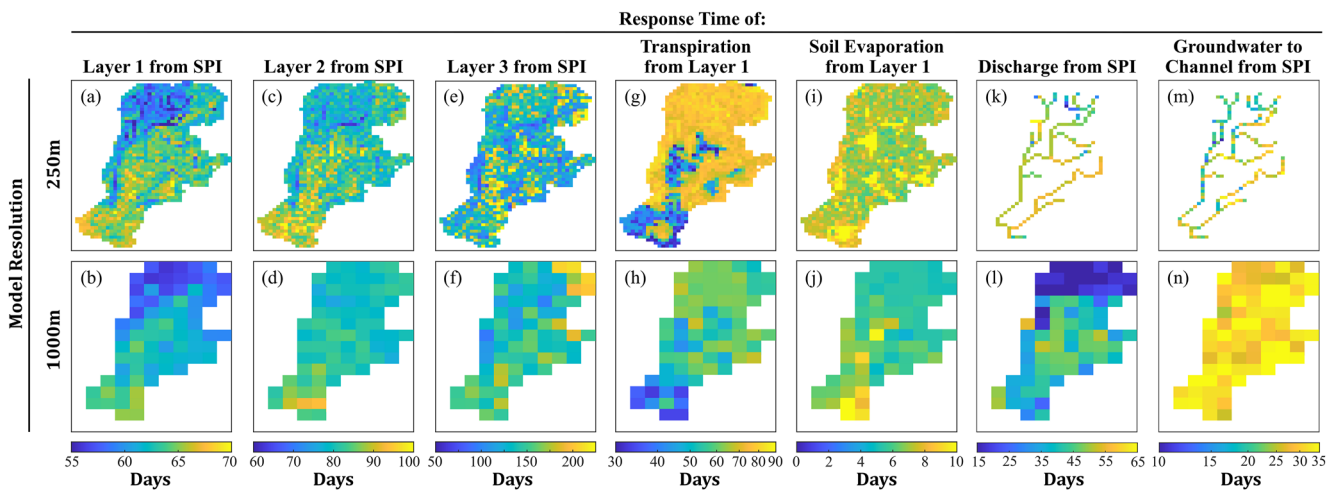

Figure 6. Average response time between precipitation or soil moisture anomalies and catchment storage and flux anomalies for 250 and 1,000 m model resolutions (all resolutions shown in Figure S8 in Supporting Information S1). The presented response time was averaged from 30, 90, and 180 days (spatial patterns are consistent). Transpiration and soil evaporation response time is presented here relative to layer 1 due to the high dependence of transpiration on soil moisture. Note that the response time of transpiration and groundwater to channel relative to SPI peak/trough is in log-scale, and groundwater storage is equivalent to Layer 3.

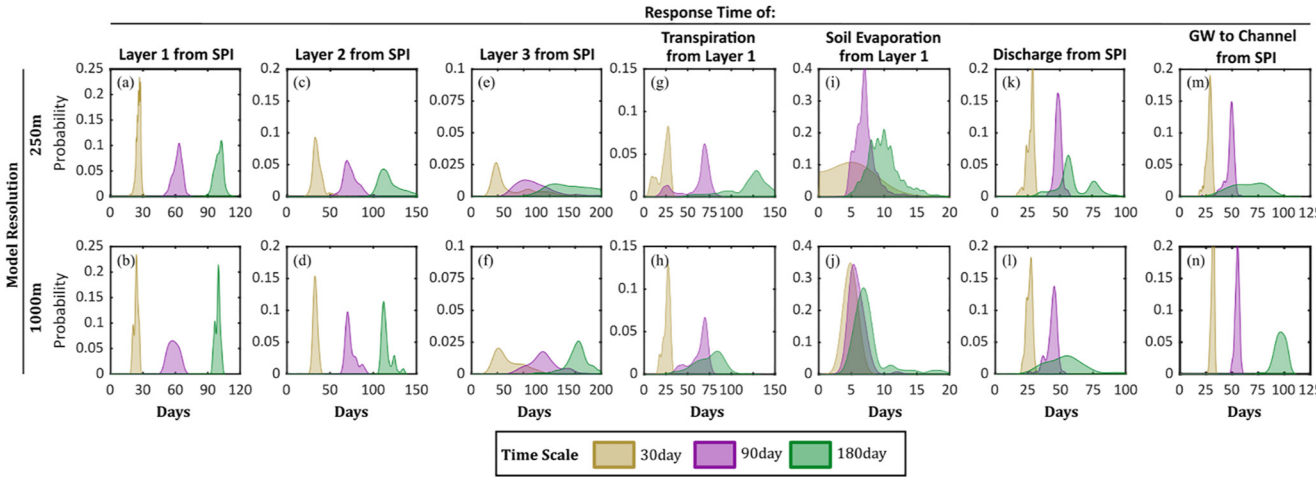

Figure 7. Distributions of estimated response time across the DMC for each time scale and 250 and 1,000 m model resolutions. All model resolutions are shown in Figure S9 in Supporting Information S1. Higher probabilities indicate a more frequent occurrence of estimated response time within the catchment and wider distributions indicate increased spatial variability.

Figure 7 shows the probability density distributions of RTs throughout the catchment (probability of occurrence in a model cell) and reveals the influence of time-scale and spatial resolution on the RT in storage and fluxes. Higher probabilities (narrower distribution) indicate lower spatial variability and mean distribution values indicate how catchment-average RTs change with time-scale (Figure 7). The RTs of all soil storages were influenced by the model spatial resolution and time scale. Greater spatial variability with deeper soil depths generally resulted in lower probabilities relative to shallower soil depths. Increased model spatial resolution generally showed decreased spatial variability (increased probabilities), while longer time-scales generally increased spatial variability (decrease probabilities). However, the general decrease in RT probability distribution was not consistent for all fluxes and storage with the 90-day time-scale (e.g., Layer 1 and 2, and soil evaporation). For all fluxes (transpiration, soil evaporation, discharge, and GW to channel), the increase in RT with time scale was much smaller than for soil storage. Transpiration RT was greatly affected by time scale and model spatial resolution, where coarser model scales decreased RTs and increased time scale increased spatial variability (decreased probability, Figures 7a–7f). With increasing model spatial resolution, the RT of groundwater flow became more spatially uniform (higher probability, Figures 7m and 7n).

The variability of RTs with catchment wetness was evaluated using for catchment averages for each storage and flux under different ranges of SPI (Figure 8 and Table S2 in Supporting Information S1). Since spatial patterns of RTs were consistent for each time scale, the catchment average RT for each SPI range is presented in Figure 8 (see table of values and correlation coefficients, Table S2 in Supporting Information S1). Soil storage RT generally decreased with increasing wetness, with only a slight increase at $1 < \text{SPI} < 2$ (Figure 8a). A faster decrease in RTs occurred at finer model resolutions (Table S2 in Supporting Information S1). The RT of transpiration with wetness was nonlinear, with a decrease in RT from very dry ($-2 < \text{SPI} < -1$) to average conditions ($-1 < \text{SPI} < 0$) before an increase in RT with increasing wetness (Figure 8b). As discharge and groundwater flow cease under low wetness conditions ($\text{SPI} < -1$), no results were applicable for these periods. Discharge and groundwater flow RTs changed nonlinearly with wetness and were exponentially shorter under extreme wetness ($\text{SPI} > 2$, Figure 8c). The relationships of catchment average RTs was relatively consistent across model resolutions, with only stream RTs showing a notable increase with increasing model spatial resolution (Table S2 in Supporting Information S1).

3.5. Spatio-Temporal Variability in Water Ages of Blue and Green Fluxes

The RT to precipitation anomaly was often very different (by orders of magnitude) from the average water ages for each storage and flux, regardless of the wetness conditions within the catchment (Figures 8 and 9). Water age in storage decreased as the wetness increased (p-value < 0.01 for layers 1 and 2). While there was a decrease in deeper soil water age with higher wetness (Figure 9a), higher model uncertainty meant this decrease was not

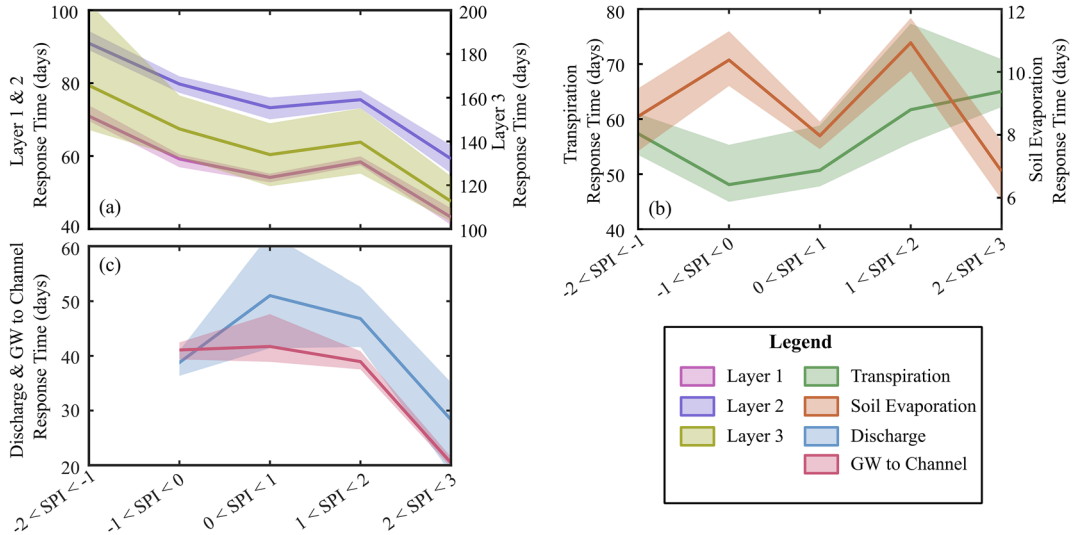

Figure 8. Catchment average of the response time of (a) soil storage, (b) transpiration and soil evaporation (with respect to Layer 1), and (c) stream water and groundwater to channel in different ranges of standardized precipitation index. Bounds represent the maximum and minimum from all model resolutions.

significant (p-value > 0.05, values and standard deviations, Table S3 in Supporting Information S1). As soil evaporation only originated from layer 1, the ages and trends were the same (Figures 9a and Figures 9b). Transpiration water age decreased nonlinearly with increasing wetness conditions (p-value < 0.01). However, unlike soil storage, transpiration water age decreased less when the catchment was wettest (SPI > 2, Figure 9b). Water age in streams generally decreased with wetness conditions; however, high uncertainty and old water ages resulted in insignificant trends in more than 50% of the stream cells for coarser resolutions (>500 m). While there were order of magnitude differences between the RTs and water ages and between model resolutions, there were relatively consistent relationships between RT and water ages (Figures 8 and 9, and Table S4 in Supporting Information S1). Strong positive linear relationships (mean $R^2 = 0.74$) were present for soil storage, with nonlinearities in the RTs and water ages of transpiration and discharge resulting in weak linear relationships (mean $R^2 = 0.21$).

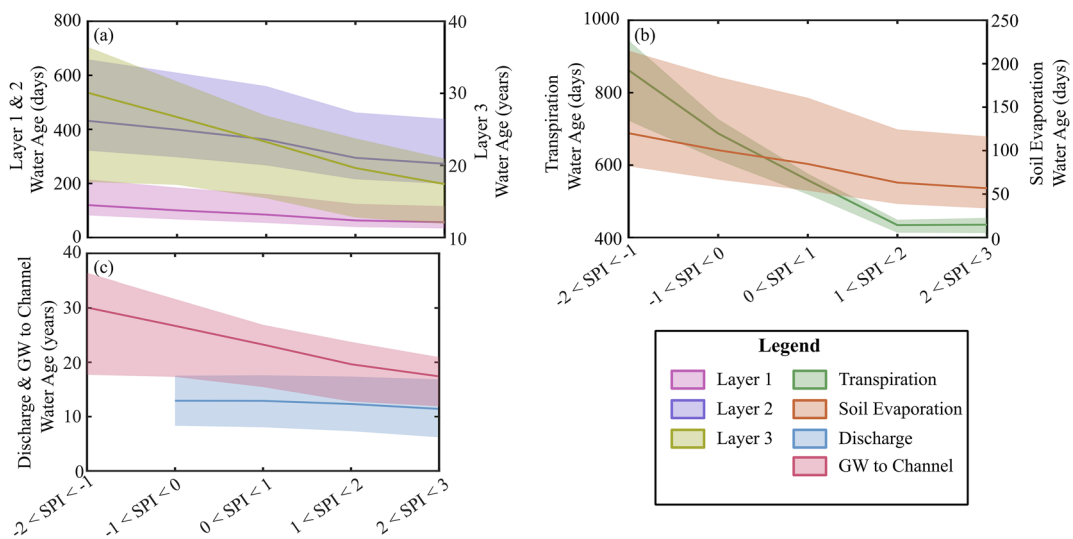

Figure 9. Catchment average of water age estimated in EcH$_2$O-iso of (a) soil storage, (b) transpiration and soil evaporation, and (c) stream water and groundwater to channel in different ranges of standardized precipitation index. Results are average values of time scale results. Bounds represent the maximum and minimum from all model resolutions. The age of groundwater to channel is equivalent to Layer 3 water age.

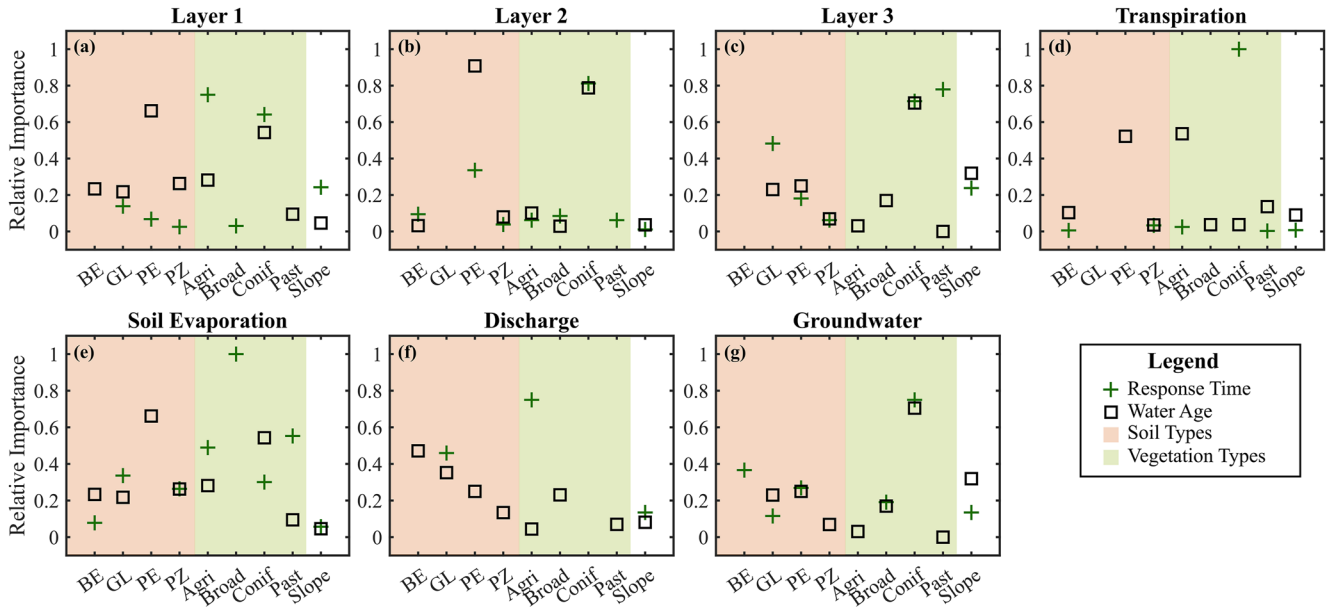

Figure 10. The relative importance of the proportion of different soils (BE, brown earth; GL, gley; PE, peat; PZ, podzol), vegetation (Agri, agricultural lands; Broad, broadleaf forest; Conif, conifer forest; Past, pastureland), and the average cell slope for the estimated response time and water age. Soils and vegetation without symbols were not significant (p-value < 0.05) to spatially explain the response time and water age.

The differences between water ages and the RTs were not solely limited to the magnitude shown by the greater divergence of RT and age with deeper soil depths (Figures 8 and 9) but also exhibited differing spatial controls (Figure 10). Stepwise multi-variate regression revealed differences in the controls of landscape features on the RTs and water ages. In shallow soils, spatial variability of water age and RT primarily corresponded to the proportion of peat soils or conifer forests, and agricultural lands or conifer forests, respectively. In deeper soils, the proportion of conifer forests had on average the strongest spatial agreement with both RT and water age (Figure 10c). For transpiration, the map of the proportion of conifers corresponded well with the spatial variability of RT, while the maps of proportions of peat soil and agricultural lands overlaid well with water ages (Figure 10d). The RT of soil evaporation was spatially correlated to the proportions of vegetation ($R^2 = 0.62$, Figure 10e). In discharge, faster RTs were mostly explained by a higher proportion of agricultural land, while spatial variability of water ages generally corresponded mostly to different soil units, with shorter ages associated with the more gleyed soils (Figure 10f). Lastly, for groundwater flow, longer ages were associated with a higher proportion of conifers and average cell slope (decreasing age with increasing slope), while higher conifer proportions dominated the control on RTs, making them longer (Figure 10g).

4. Discussion

4.1. How Does Spatio-Temporal Variability of Catchment Storages and Fluxes Modulate Various Wetness Conditions?

Advances in ecohydrological modelling have facilitated further evaluation of landscape-scale soil-vegetation linkages in space and time by distinguishing storages and fluxes of soil and vegetation water pools (Asbjornsen et al., 2011). Through examination of the temporal and spatial variability of catchment storage and flux dynamics, modelling results provide additional insights into integrated catchment function under hydroclimatic perturbations in terms of blue and green water fluxes (Rodriguez-Iturbe, 2000).

During changing wetness conditions, especially re-wetting, we found a high degree of spatio-temporal variability in both storage and flux dynamics that was strongly linked to the proportions of different vegetation and soil units. Land use in particular had a large role in distinguishing spatial differences of soil storages and green water flux dynamics (Figure 4). While both northern and southern areas in the DMC are dominated by silty brown earth soils (Figure 1), land use is agriculture and conifer forests, respectively. Despite similar underlying soils, there was large spatial variability in the sensitivity of soil moisture to catchment wetness between the North and South

which was mostly driven by land cover type, similar to other regions in Germany (Korres et al., 2015). Thus, land use and vegetation species characteristics have a key role in modulating the temporal variability of groundwater recharge throughout this drought-sensitive region, where decreases in groundwater recharge have more acute significance for ecosystem services than in other regions (Schwaiger et al., 2019). The higher sensitivity of soil moisture to catchment wetness in the conifer forests, coupled with potential long-term decreases in summer precipitation in Germany (Hansel et al., 2009) will likely result in reductions to the already low groundwater recharge during the summer (Douinot et al., 2019; Smith, Tetzlaff, Kleine, et al., 2020). Wetland soil moisture, particularly in the deeper soils, was the least sensitive to hydroclimatic perturbations, which corresponds to the coupled lower total green water usage and transpiration previously estimated (Smith et al., 2021). This suggests that blue water movement, including flow attenuation provided by wetlands (e.g., Blanchette et al. (2019)) and low topographic relief (Figure 1a) will have increasing importance in moderating the temporal variability of water storage in the catchment. Spatial variability of precipitation during re-wetting periods may also drive some spatial differences in soil moisture sensitivity to wetness (Maneta et al., 2018); however, the dominance of ET water use in the catchment (~90% of precipitation) likely limits the importance of precipitation-induced spatial variability. The results in the catchment have wider implications for larger regions of managed landscapes, where careful consideration of land use strategies via vegetation type may help mitigate climatic extremes. Through careful siting and zoning, the distribution of crops, grasslands, and wetlands to maintain groundwater levels and streamflow, or forests to reduce runoff in wetter periods regions of low and high projections of climatic precipitation, respectively. Furthermore, the low sensitivity of wetlands to hydroclimatic perturbations in the catchment could highlights the importance of further maintaining and rehabilitating wetlands as hydrologic buffers in regions where precipitation is projected to decrease.

Similarly to the spatio-temporal sensitivity of soil moisture to catchment wetness, the temporal sensitivity of both blue and green water fluxes to catchment wetness were spatially correlated with land use (Figures 1 and 4). While spatial patterns of increases in transpiration with wetness conditions unsurprisingly showed clear influences of land use, the magnitude of increase revealed differing temporal functionality of land cover (Figure 4). Although layer 1 moisture increased more with higher precipitation anomalies in the agricultural areas, transpiration increased more in the conifer forests despite high root-uptake proportions from near-surface soil water under both agriculture and forests (Smith et al., 2021). This contrasting response between vegetation types is the result of a difference in the degree to which soil moisture stress and atmospheric demand and vapour pressure deficit (VPD) regulate water losses in the conifer forests and agricultural areas, respectively (Figures 5a,5b,5e, and 5f). This sensitivity has been also observed at subcontinental scales using remote sensing-based estimations of ET (Brust et al., 2021). A decrease in summer precipitation may increase VPD and moisture stress, likely resulting in a larger decrease in forest transpiration (moisture limited) than agricultural areas (Figures 5a,5b,5e, and 5f). The magnitude of temporal dynamics of soil evaporation was moderated to a large extent by the spatial proportions of wetlands (Figures 1, 4i, and 4j). Higher wetland evaporation is consistent with patterns found in other tracer studies (Sprenger et al., 2017; Welch et al., 2018). Temporal patterns of discharge and flow generation (groundwater to channel fluxes) followed a nonlinear increase with catchment wetness (e.g., Kirchner 2009) (Figures 4k–4n, and Figure S2 in Supporting Information S1); however, the relationships between land cover and discharge, and land cover and groundwater flow were not as clear as for other storages and fluxes. Spatial variability but temporal persistence of internal catchment flow mechanisms (e.g., internal flow paths driven by time-invariant topography; Maneta et al. (2018)), channel evaporation (Smith et al., 2021), and potentially the anthropogenic impacts on the channel network may have obscured more clear correlations between land cover and discharge (or groundwater flow). The incised stream network may have resulted in better drainage and reduced groundwater to stream connectivity, which is observed by the groundwater inflows to the channel in locations where anthropogenic influences were smaller and coincide with locations of the historic channel network (Gelbrecht et al., 2005).

4.2. How Do Spatio-Temporal Dynamics of Water Age and Response Time of Storages and Fluxes Vary With Hydroclimatic Perturbations?

Accurate model representation of internal fluxes and storages provide insights into catchment hydrological function (Kirchner, 2006). Modelled water age (as a proxy for particle velocities) and hydrological RTs (as a proxy for celerity) provide two distinct perspectives from which to interpret catchment hydrologic response. In combination, water age and RTs provide a framework to understand the rapid movement of old water following rainfall

inputs to a catchment (Kirchner, 2003), and to test hypotheses of spatio-temporal catchment dynamics across scales (McDonnell & Beven, 2014).

Modelled water age and RTs showed significant temporal variability with hydroclimatic perturbations, with a general decline in RT as catchment wetness increased for all catchment storages (increase in RT only when $1 < SPI < 2$, Figures 8a and 9a). This decrease in RTs with increasing wetness was spatially consistent regardless of vegetation or soil unit (Figures 4a–4f). This is consistent with the expected direct correlation of celerity times with storage deficits (Beven, 2020) and with expected changes with antecedent conditions (Davies & Beven, 2015). Similarly, the tendency of decreasing water ages in storage with increasing wetness is in line with other studies (Beven & Davies, 2015; van Huijgevoort et al., 2016). Furthermore, differences between the water age and RT as shown by the ratio of water age to RT (Table S4 in Supporting Information S1) had a general tendency to decrease with increasing wetness similar to other studies (e.g., Beven, (2020)), though this is statistically insignificant due to large water age uncertainty. However, the limited variability of simulated storage response and water ages with wetness conditions was not anticipated (Table S3 and Figure S2 in Supporting Information S1). The effect of storage averaging with larger catchment scale (e.g., Davies and Beven (2015)), dependencies on mixing (e.g., Fenicia et al. (2010)) as well as fewer periods of higher wetness conditions may contribute to the damped nonlinearity. Spatially, the RTs were the longest in the drier forest dominated southern areas. These areas also had the greatest largest difference of water age from RT due to greater prevalence of older water ages which further progressed through the soil (Figure S10 in Supporting Information S1). While increased RT with propagation through soils is anticipated (Van Loon, 2015), the high dependence of forests on soil moisture and greater total evapotranspiration (Smith et al., 2021) was likely the reason for the increased RT of the soils (Struthers et al., 2006) and older water ages in recharge (underlining the importance of forests in Figure 10).

The nonlinearity of the RT with wetness conditions was more apparent for transpiration, discharge, and groundwater fluxes in both space and time (Figures 8b and 8c). Despite notable spatial differences in the soil response due to hydroclimatic perturbations, which shows both a faster and greater response in the agricultural areas, the transpiration RT is spatially more dependent on whether the vegetation is regulated by soil moisture stress or VPD (Figure 10d). This relationship may work in conjunction with the soil RTs, where the faster-responding transpiration delays the recovery from drought in deeper storage (e.g., Van Loon (2015)) and increases the total RT of soils. In discharge, a relatively consistent decrease in water age occurred as wetness increased (Figure 9c), reflecting the inverse storage effect (Harman, 2015). In conjunction, the nonlinear decrease in RT with increasing wetness (Figure 8c) resulted in a larger separation of water age from RT with increasing wetness and reflects the old water paradox during larger events (Kirchner, 2003). Spatial patterns reflected shorter RTs in the northern, slightly steeper, areas of the catchment, which is consistent with the effect of a hydraulic gradient on RTs (Beven, 2020). Conversely, the discharge RT decreased as wetness increased and responded faster than soil storage, similar to other regions (e.g., Andreadis et al. (2005)). However, higher uncertainty coupled with relatively old water and limited periods of high wetness precluded any significant change in modelled discharge age with SPI.

The spatio-temporal differences in RT and water ages observed in the catchment may have significant implications at larger scales under long-term climate change projections. The increase in both the RT and water age under dry conditions implies that nutrient and contaminant transport rapidly decreases and extends the timescale required for natural mitigation strategies, such as modification of the timing and quantity of fertilizer application under projections of lower precipitation.

4.3. What Is the Influence of Model Resolution on Perceived Spatiotemporal Correlations and Catchment Responsiveness?

The nature of dominant modelled processes and flow paths are highly dependent on model spatial resolution, with coarser scales aggregating processes to reproduce point (discharge) or spatial averages (catchment average evapotranspiration) of fluxes. Process aggregation and the accompanying general shift from nonlinearity toward linear responses as grid scales increase (Figure S2 in Supporting Information S1) (Sivapalan et al., 2002) causes difficulties in interpreting modelled results across scales. The evaluation of storages and fluxes, water ages, and RT helped identify the influence of model grid resolution on spatio-temporal patterns. At larger scales (750 and 1000 m cell sizes) the extreme high and low increases in soil moisture with wetness conditions for all soil layers were apparent, with decreased obvious visual links to catchment features (soil and vegetation) similar to other upscaling studies (e.g., Samaniego et al. (2017)). The effect of upscaling on soil moisture dynamics, and the

corresponding higher average total stored water with increasing model spatial resolution (Smith et al., 2021) was not limited only to moisture but was also present for the RT of soils. A similar effect of spatial averaging of RT with increasing model scales has been observed in other studies (e.g., Davies and Beven (2015)). The most notable differences between model scales—including fluxes, storages, water ages, and RTs—was with transpiration, discharge, and groundwater flow to channels (Figures 4–6). In particular, the lower dependence of transpiration on soil moisture (Figure 5, and Figures S5 and S6 in Supporting Information S1) at coarser scales for much of the catchment is likely linked to the limitation of spatial variability in soil moisture, which would be necessary to drive water fluxes from the soil (Vereecken et al., 2008). With the soil RT, a notable scaling effect was observed between the 500 and 750 m model resolutions, with much faster RTs in channel cells through layers 1 and 2 (Figure S8 in Supporting Information S1). Davies and Beven (2015) observed a similar result with a gradual loss of channel influence caused by increased average moisture with scale and increased resolution and more averaged response over the catchment as a result of slower draining. The increasing linearization of discharge and groundwater flow with spatial resolution was clearly present through the evaluation of fluxes and RTs under different wetness conditions (Figures 4k–4n, 6k–6n, and Figure S2 in Supporting Information S1) and observed in catchment draining patterns in catchment-aggregated studies (Maneta et al., 2018). Similar to the spatial resolution limit on soil RTs, the linearization becomes more marked at scales above 500 m, suggesting a limitation in the runoff process representation (Blöschl & Sivapalan, 1995). This linkage of the resolution, RT, and flux and storage is of great value as it simultaneously demonstrates boundary limits of model use for hypothesis testing. This also underlines the insights from the use of tracer aided models where these interactions can be constrained by isotope-based calibration.

5. Conclusion

Evaluation of the spatio-temporal variability in fluxes, storage, and water age and response times due to hydroclimatic perturbations is essential to make inferences about complex internal catchment processes and exiting flow paths. Based on the robust multi-criteria calibration of a tracer-aided ecohydrologic model, we explored internal catchment hydrologic mechanisms across spatial scales and different temporal periods with varying fluxes and storage dynamics, as well as contrasting water age and response times (RTs). The results demonstrate the key role of vegetation in mediating hydroclimatic perturbations to storage and flux dynamics in response to both short and long-term hydroclimatic anomalies. Transpiration had a spatially variable response to precipitation perturbations (Figure S2 in Supporting Information S1), with spatial differences in vegetation units exhibiting different degrees of soil moisture-regulated transpiration and vapour deficit-regulated transpiration. The heterogeneous controls on transpiration regulate the spatial sensitivity of soil moisture to precipitation anomalies. RTs showed strong spatial connections to land cover units, with faster-responding soil moisture and discharge in agricultural areas and faster-responding transpiration in conifer forests. The fast RTs of transpiration resulted in greater spatial variability in the separation of water age from RT in shallow soils, and play a key role in the larger spatial variability in the difference of RTs from water ages in deeper soils. The rapid propagation of RT through soils largely resulted in an exponential increase in the separation from water ages along the flow paths, thereby causing large differences between discharge and groundwater ages and their relatively short respective RTs. Hydroclimatic perturbations were a primary cause for temporal variability of RTs and water age, with generally shorter RTs and younger water ages with higher precipitation anomalies. Spatial variability of storage-flux, and RT and water age interactions were aggregated with coarsening model resolution, resulting in the loss of identifiable "hot spots" during the aggregation process. This resulted in a different combination of salient factors modulating catchment fluxes and storages, and a disproportionate increase in change in the relationship between RT and water age. The spatio-temporal dependencies on hydroclimatic perturbations revealed in this study provides a window to explore internal catchment dynamics and shows that our perception of catchment function is scale-dependent. It also provides a practical example of the effectiveness of evaluating interactions of velocity and celerity or their proxies to further understand landscape-scale vegetation-soil interactions.

Data Availability Statement

The model code of EcH2O-iso is available at http://bitbucket.igb-berlin.de:7990/users/ech2o/repos/ech2o_iso/browse. Data used in this study were presented in Smith et al., 2021, https://doi.org/10.5194/hess-25-2239-2021.

Acknowledgments
The authors acknowledge funding from the European Research Council (Grant No. GA 335910 VeWa). Contributions from CS were supported by the Leverhulme Trust through the ISO-LAND project (Grant No. RPG 2018 375). Isotopic analysis was conducted by David Dubbert at the Leibniz-Institute of Freshwater Ecology and Inland Fisheries. The authors acknowledge the University of Aberdeen IT services for the use of the high-performance computing (HPC cluster), which was used for all model runs. Funding for DT was also received through the Einstein Research Unit "Climate and Water under Change" from the Einstein Foundation Berlin and Berlin University Alliance.

References

Ahmed, K. R., Paul-Limoges, E., Rascher, U., & Damm, A. (2020). A first assessment of the 2018 European drought impact on ecosystem evapotranspiration. *Remote Sensing*, *13*(1). https://doi.org/10.3390/rs13010016

Ameli, A. A., Amvrosiadi, N., Grabs, T., Laudon, H., Creed, I. F., McDonnell, J. J., & Bishop, K. (2016). Hillslope permeability architecture controls on subsurface transit time distribution and flow paths. *Journal of Hydrology*, *543*, 17–30. https://doi.org/10.1016/j.jhydrol.2016.04.071

Andreadis, K., Clark, E., Wood, A., Hamlet, A., & Lettenmaier, D. (2005). Twentieth-century drought in the conterminous United States. *American Meteorological Society*, *6*, 985–1001. https://doi.org/10.1175/jhm450.1

Asbjornsen, H., et al. (2011). Ecohydrological advances and applications in plant-water relations research: A review. *Journal of Plant Ecology*, *4*(1–2), 3–22. https://doi.org/10.1093/jpe/rtr005

Botter, G., Bertuzzo, E., & Rinaldo, A. (2010). Transport in the hydrologic response: Travel time distributions, soil moisture dynamics, and the old water paradox. *Water Resources Research*, *46*, W03514. https://doi.org/10.1029/2009WR008371

Beven, K. (2020). A history of the concept of time of concentration. *Hydrology and Earth System Sciences*, *24*(5), 2655–2670. https://doi.org/10.5194/hess-24-2655-2020

Beven, K., & Davies, J. (2015). Velocities, celerities and the basin of attraction in catchment response. *Hydrological Processes*, *29*(25), 5214–5226. https://doi.org/10.1002/hyp.10699

Birkel, C., Soulsby, C., Tetzlaff, D., Dunn, S., & Spezia, L. (2012). High-frequency storm event isotope sampling reveals time-variant transit time distributions and influence of diurnal cycles. *Hydrological Processes*, *26*(2), 308–316. https://doi.org/10.1002/hyp.8210

Blanchette, M., Rousseau, A. N., Foulon, E., Savary, S., & Poulin, M. (2019). What would have been the impacts of wetlands on low flow support and high flow attenuation under steady state land cover conditions? *Journal of Environmental Management*, *234*, 448–457. https://doi.org/10.1016/j.jenvman.2018.12.095

Blöschl, G., & Sivapalan, M. (1995). Scale issues in hydrological modelling: A review. *Hydrological Processes*, *9*, 251–290. https://doi.org/10.1002/hyp.3360090305

Box, G. E. P., Jenkins, G. M., & Reinsel, G. C. (1994). *Time series analysis: Forecasting and control* (3rd ed.). Prentice Hall.

Brewer, S. K., Worthington, T. A., Mollenhauer, R., Stewart, D. R., McManamay, R. A., Guertault, L., & Moore, D. (2018). Synthesizing models useful for ecohydrology and ecohydraulic approaches: An emphasis on integrating models to address complex research questions. *Ecohydrology*, *11*(7). https://doi.org/10.1002/eco.1966

Brust, C., Kimball, J. S., Maneta, M. P., Jencso, K., He, M., & Reichle, R. H. (2021). *Using SMAP Level-4 soil moisture to constrain MOD16 evapotranspiration over the contiguous USA* (p. 255). Remote Sensing of Environment.

Danesh-Yazdi, M., Klaus, J., Condon, L. E., & Maxwell, R. M. (2018). Bridging the gap between numerical solutions of travel time distributions and analytical storage selection functions. *Hydrological Processes*, *32*(8), 1063–1076. https://doi.org/10.1002/hyp.11481

Dari, J., Morbidelli, R., Saltalippi, C., Massari, C., & Brocca, L. (2019). Spatial-temporal variability of soil moisture: Addressing the monitoring at the catchment scale. *Journal of Hydrology*, *570*, 436–444. https://doi.org/10.1016/j.jhydrol.2019.01.014

Davies, J., & Beven, K. (2015). Hysteresis and scale in catchment storage, flow and transport. *Hydrological Processes*, *29*(16), 3604–3615. https://doi.org/10.1002/hyp.10511

Douinot, A., Tetzlaff, D., Maneta, M., Kuppel, S., Schulte-Bisping, H., & Soulsby, C. (2019). Ecohydrological modelling with EcH$_2$O-iso to quantify forest and grassland effects on water partitioning and flux ages. *Hydrological Processes*.

Dubbert, M., & Werner, C. (2019). Water fluxes mediated by vegetation: Emerging isotopic insights at the soil and atmosphere interfaces. *New Phytologist*, *221*(4), 1754–1763. https://doi.org/10.1111/nph.15547

DWD. (2021). *CDC (Climate Data Center)*, edited.

ECMWF. (2021). *ERA5-Land hourly data from 1981 to present*, edited.

Fatichi, S., Pappas, C., & Ivanov, V. Y. (2015). Modeling plant–water interactions: An ecohydrological overview from the cell to the global scale. *WIREs Water*, *3*(3), 327–368. https://doi.org/10.1002/wat2.1125

Fenicia, F., Wrede, S., Kavetski, D., Pfister, L., Hoffmann, L., Savenije, H. H. G., & McDonnell, J. J. (2010). Assessing the impact of mixing assumptions on the estimation of streamwater mean residence time. *Hydrological Processes*, *24*(12), 1730–1741. https://doi.org/10.1002/hyp.7595

Frigo, M., & Johnson, S. G. (1998). *FFTW: An adaptive software architecture for the FFT. Paper Presented at International Conference on Acoustics, Speech, and signal processing*.

Gelbrecht, J., Driescher, E., Lademann, H., Schonfelder, J., et al. (1996). Diffuse nutrient impact on surface water bodies and its abatement by restoration measures in a small catchment area in north-east Germany. *Water Science and Technology*, *33*(4–5), 167–174. https://doi.org/10.2166/wst.1996.0501

Gelbrecht, J., Lengsfeld, H., Pöthig, R., & Opitz, D. (2005). Temporal and spatial variation of phosphorus input, retention and loss in a small catchment of NE Germany. *Journal of Hydrology*, *304*(1–4), 151–165. https://doi.org/10.1016/j.jhydrol.2004.07.028

Guse, B., Pfannerstill, M., Kiesel, J., Strauch, M., Volk, M., & Fohrer, N. (2019). Analysing spatio-temporal process and parameter dynamics in models to characterise contrasting catchments. *Journal of Hydrology*, *570*, 863–874. https://doi.org/10.1016/j.jhydrol.2018.12.050

Guswa, A. J., et al. (2020). Advancing ecohydrology in the 21st century: A convergence of opportunities. *Ecohydrology*, *13*(4). https://doi.org/10.1002/eco.2208

Gutzler, C., Helming, K., Balla, D., Dannowski, R., Deumlich, D., Glemnitz, M., et al. (2015). Agricultural land use changes—A scenario-based sustainability impact assessment for Brandenburg, Germany. *Ecological Indicators*, *48*, 505–517. https://doi.org/10.1016/j.ecolind.2014.09.004

Hansel, S., Petzold, S., & Matschullat, J. (2009). *Bioclimatology and natural hazards*. In K. Střelcová, C. Mátyás, A. Kleidon, M. Lapin, F. Matejka, M. Blaženec, J. Škvarenina, & J. Holécy (Eds.).

Harman, C. J. (2015). Time-variable transit time distributions and transport: Theory and application to storage-dependent transport of chloride in a watershed. *Water Resources Research*, *51*(1), 1–30. https://doi.org/10.1002/2014wr015707

Harman, C. J. (2019). Age-ranked storage-discharge relations: A unified description of spatially lumped flow and water age in hydrologic systems. *Water Resources Research*, *55*(8), 7143–7165. https://doi.org/10.1029/2017wr022304

Holmes, T., Stadnyk, T. A., Kim, S. J., & Asadzadeh, M. (2020). Regional calibration with isotope tracers using a spatially distributed model: A comparison of methods. *Water Resources Research*, *56*(9). https://doi.org/10.1029/2020wr027447

King, A. D., & Karoly, D. J. (2017). Climate extremes in Europe at 1.5 and 2 degrees of global warming. *Environmental Research Letters*, *12*(11). https://doi.org/10.1088/1748-9326/aa8e2c

Kirchner, J. W. (2003). A double paradox in catchment hydrology and geochemistry. *Hydrological Processes*, *17*(4), 871–874. https://doi.org/10.1002/hyp.5108

Kirchner, J. W. (2006). Getting the right answers for the right reasons: Linking measurements, analyses, and models to advance the science of hydrology. *Water Resources Research*, *42*(3). https://doi.org/10.1029/2005wr004362
Kirchner, J. W. (2009). Catchments as simple dynamical systems: Catchment characterization, rainfall-runoff modeling, and doing hydrology backward. *Water Resources Research*, *45*(2). https://doi.org/10.1029/2008wr006912
Kirchner, J. W., Feng, X., & Neal, C. (2000). Fractal stream chemistry and its implications for contaminant transport in catchments. *Nature*, *403*, 524–527. https://doi.org/10.1038/35000537
Kleine, L., Tetzlaff, D., Smith, A., Goldhammer, T., & Soulsby, C. (2021). Intermittent flows in a lowland, groundwater-dominated, mixed land-use catchment: An isotopic approach to understanding droughts. *Hydrological Processes*.
Kleine, L., Tetzlaff, D., Smith, A., Wang, H., & Soulsby, C. (2020). Using water stable isotopes to understand evaporation, moisture stress, and re-wetting in catchment forest and grassland soils of the summer drought of 2018. *Hydrology and Earth System Sciences*, *24*(7), 3737–3752. https://doi.org/10.5194/hess-24-3737-2020
Köplin, N., Schädler, B., Viviroli, D., & Weingartner, R. (2012). Relating climate change signals and physiographic catchment properties to clustered hydrological response types. *Hydrology and Earth System Sciences*, *16*(7), 2267–2283. https://doi.org/10.5194/hess-16-2267-2012
Korres, W., Reichenau, T. G., Fiener, P., Koyama, C. N., Bogena, H. R., Cornelissen, T., et al. (2015). Spatio–temporal soil moisture patterns—A meta-analysis using plot to catchment scale data. *Journal of Hydrology*, *520*, 326–341. https://doi.org/10.1016/j.jhydrol.2014.11.042
Kuppel, S., Tetzlaff, D., Maneta, M. P., & Soulsby, C. (2018). EcH2O-iso 1.0: Water isotopes and age tracking in a process-based, distributed ecohydrological model. *Geoscientific Model Development*, *11*(7), 3045–3069. https://doi.org/10.5194/gmd-11-3045-2018
Kuppel, S., Tetzlaff, D., Maneta, M. P., & Soulsby, C. (2020). Critical zone storage controls on the water ages of ecohydrological outputs. *Geophysical Research Letters*, *47*(16). https://doi.org/10.1029/2020gl088897
Lee, T. (2021). *Standardized precipitation index edited*. MATLAB Central File Exchange.
LfU, Landesamt für Umwelt. (2019). Ministry of rural development, *environment and agriculture of the federal state of Brandenburg*. Retrieved from https://mlul.brandenburg.de/cms/detail.php/bb1.c.288254.de
Lorenz, R., Stalhandske, Z., & Fischer, E. M. (2019). Detection of a climate change signal in extreme heat, heat stress, and cold in Europe from observations. *Geophysical Research Letters*, *46*(14), 8363–8374. https://doi.org/10.1029/2019gl082062
Maneta, M. P., & Silverman, N. L. (2013). A spatially distributed model to simulate water, energy, and vegetation dynamics using information from regional climate models. *Earth Interactions*, *17*(11), 1–44. https://doi.org/10.1175/2012ei000472.1
Maneta, M. P., Soulsby, C., Kuppel, S., & Tetzlaff, D. (2018). Conceptualizing catchment storage dynamics and nonlinearities. *Hydrological Processes*. https://doi.org/10.1002/hyp.13262
Marx, A., Kumar, R., Thober, S., Rakovec, O., Wanders, N., Zink, M., et al. (2018). Climate change alters low flows in Europe under global warming of 1.5, 2, and 3°C. *Hydrology and Earth System Sciences*, *22*(2), 1017–1032. https://doi.org/10.5194/hess-22-1017-2018
McDonnell, J. J., & Beven, K. (2014). Debates-the future of hydrological sciences: A (common) path forward? A call to action aimed at understanding velocities, celerities and residence time distributions of the headwater hydrograph. *Water Resources Research*, *50*(6), 5342–5350. https://doi.org/10.1002/2013wr015141
McKee, T., Doesken, N., & Kleist, J. (1993). The relationship of drought frequency and duration to time scales. In *Eighth Conference on applied Climatology*, edited.
Morris, M. (1991). Factorial sampling plans for preliminary computational experiments. *Technometrics*, *33*(2), 161–174. https://doi.org/10.1080/00401706.1991.10484804
Okruszko, T., Duel, H., Acreman, M., Grygoruk, M., Flörke, M., & Schneider, C. (2011). Broad-scale ecosystem services of European wetlands—Overview of the current situation and future perspectives under different climate and water management scenarios. *Hydrological Sciences Journal*, *56*(8), 1501–1517. https://doi.org/10.1080/02626667.2011.631188
Orth, R., & Destouni, G. (2018). Drought reduces blue-water fluxes more strongly than green-water fluxes in Europe. *Nature Communications*, *9*(1), 3602. https://doi.org/10.1038/s41467-018-06013-7
Pangle, L. A., Kim, M., Cardoso, C., Lora, M., Meira Neto, A. A., Volkmann, T. H. M., et al. (2017). The mechanistic basis for storage-dependent age distributions of water discharged from an experimental hillslope. *Water Resources Research*, *53*(4), 2733–2754. https://doi.org/10.1002/2016wr019901
Piovano, T., Tetzlaff, D., Maneta, M., Buttle, J. M., Carey, S. K., Laudon, H., et al. (2020). Contrasting storage-flux-age interactions revealed by catchment inter-comparison using a tracer-aided runoff model. *Journal of Hydrology*, *590*. https://doi.org/10.1016/j.jhydrol.2020.125226
Rinaldo, A., Beven, K. J., Bertuzzo, E., Nicotina, L., Davies, J., Fiori, A., et al. (2011). Catchment travel time distributions and water flow in soils. *Water Resources Research*, *47*, W07537. https://doi.org/10.1029/2011WR010478
Rodriguez-Iturbe, I. (2000). Ecohydrology: A hydrologic perspective of climate-soil-vegetation dynamics. *Water Resources Research*, *36*(1), 3–9. https://doi.org/10.1029/1999wr900210
Running, S., Mu, Q., & Zhao, M. (2017). In N. E. L. P. DAAC (Ed.), *MOD16A2 MODIS/Terra net evapotranspiration 8-day L4 Global 500m SIN Grid V006*.
Samaniego, L., Kumar, R., Thober, S., Rakovec, O., Zink, M., Wanders, N., et al. (2017). Toward seamless hydrologic predictions across spatial scales. *Hydrology and Earth System Sciences*, *21*(9), 4323–4346. https://doi.org/10.5194/hess-21-4323-2017
Schwaiger, F., Poschenrieder, W., Biber, P., & Pretzsch, H. (2019). Ecosystem service trade-offs for adaptive forest management. *Ecosystem Services*, *39*. https://doi.org/10.1016/j.ecoser.2019.100993
Shekhar, A., Chen, J., Bhattacharjee, S., Buras, A., Castro, A. O., Zang, C. S., & Rammig, A. (2020). Capturing the impact of the 2018 European drought and heat across different vegetation types using OCO-2 solar-induced fluorescence. *Remote Sensing*, *12*(19). https://doi.org/10.3390/rs12193249
Sivapalan, M., Jothityangkoon, C., & Menabde, M. (2002). Linearity and nonlinearity of basin response as a function of scale: Discussion of alternative definitions. *Water Resources Research*, *38*(2), 4–145. https://doi.org/10.1029/2001wr000482
Smith, A., Tetzlaff, D., Gelbrecht, J., Kleine, L., & Soulsby, C. (2020). Riparian wetland rehabilitation and beaver re-colonization impacts on hydrological processes and water quality in a lowland agricultural catchment. *The Science of the Total Environment*, *699*, 134302. https://doi.org/10.1016/j.scitotenv.2019.134302
Smith, A., Tetzlaff, D., Kleine, L., Maneta, M., & Soulsby, C. (2021). Upscaling land-use effects on water partitioning and water ages using tracer-aided ecohydrological models. *Hydrology and Earth System Sciences Discussions*, *2020*, 1–36.
Smith, A., Tetzlaff, D., Kleine, L., Maneta, M. P., & Soulsby, C. (2020). Isotope-aided modelling of ecohydrologic fluxes and water ages under mixed land use in Central Europe: The 2018 drought and its recovery. *Hydrological Processes*, *34*(16), 3406–3425. https://doi.org/10.1002/hyp.13838
Sohier, H., Farges, J.-L., & Piet-Lahanier, H. (2014). Improvement of the representativity of the Morris Method for air-launch-to-orbit separation. *IFAC Proceedings Volumes*, *47*, 7954–7959

Soulsby, C., Birkel, C., Geris, J., Dick, J., Tunaley, C., & Tetzlaff, D. (2015). Stream water age distributions controlled by storage dynamics and nonlinear hydrologic connectivity: Modeling with high-resolution isotope data. *Water Resources Research*, *51*(9), 7759–7776. https://doi.org/10.1002/2015wr017888

Spinoni, J., Naumann, G., & Vogt, J. V. (2017). Pan-European seasonal trends and recent changes of drought frequency and severity. *Global and Planetary Change*, *148*, 113–130. https://doi.org/10.1016/j.gloplacha.2016.11.013

Sprenger, M., Stumpp, C., Weiler, M., Aeschbach, W., Allen, S. T., Benettin, P., et al. (2019). The demographics of water: A review of water ages in the critical zone. *Reviews of Geophysics*, *57*(3), 800–834. https://doi.org/10.1029/2018rg000633

Sprenger, M., Tetzlaff, D., Tunaley, C., Dick, J., & Soulsby, C. (2017). Evaporation fractionation in a peatland drainage network affects stream water isotope composition. *Water Resources Research*, *53*(1), 851–866. https://doi.org/10.1002/2016wr019258

Struthers, I., Hinz, C., & Sivapalan, M. (2006). A multiple wetting front gravitational infiltration and redistribution model for water balance applications. *Water Resources Research*, *42*(6). https://doi.org/10.1029/2005wr004645

Surfleet, C. G., Tullos, D., Chang, H., & Jung, I.-W. (2012). Selection of hydrologic modeling approaches for climate change assessment: A comparison of model scale and structures. *Journal of Hydrology*, *464–465*, 233–248. https://doi.org/10.1016/j.jhydrol.2012.07.012

Tetzlaff, D., Birkel, C., Dick, J., Geris, J., & Soulsby, C. (2014). Storage dynamics in hydropedological units control hillslope connectivity, runoff generation, and the evolution of catchment transit time distributions. *Water Resources Research*, *50*(2), 969–985. https://doi.org/10.1002/2013wr014147

Tetzlaff, D., Carey, S. K., McNamara, J. P., Laudon, H., & Soulsby, C. (2017). The essential value of long-term experimental data for hydrology and water management. *Water Resources Research*, *53*(4), 2598–2604. https://doi.org/10.1002/2017wr020838

Teuling, A. J., Badtsde, E. A. G., Jansen, F. A., Fuchs, R., Buitink, J., Hoek van Dijke, A. J., & Sterling, S. M. (2019). Climate change, reforestation/afforestation, and urbanization impacts on evapotranspiration and streamflow in Europe. *Hydrology and Earth System Sciences*, *23*(9), 3631–3652. https://doi.org/10.5194/hess-23-3631-2019

Huijgevoortvan , M. H. J., Tetzlaff, D., Sutanudjaja, E. H., & Soulsby, C. (2016). Using high resolution tracer data to constrain water storage, flux and age estimates in a spatially distributed rainfall-runoff model. *Hydrological Processes*, *30*(25), 4761–4778. https://doi.org/10.1002/hyp.10902

Van Loon, A. F. (2015). Hydrological drought explained. *Wiley Interdisciplinary Reviews: Water*, *2*(4), 359–392. https://doi.org/10.1002/wat2.1085

Van Loon, A. F., Kumar, R., & Mishra, V. (2017). Testing the use of standardised indices and GRACE satellite data to estimate the European 2015 groundwater drought in near-real time. *Hydrology and Earth System Sciences*, *21*(4), 1947–1971. https://doi.org/10.5194/hess-21-1947-2017

Verseveldvan , W. J., Barnard, H. R., Graham, C. B., McDonnell, J. J., Brooks, J. R., & Weiler, M. (2017). A sprinkling experiment to quantify celerity-velocity differences at the hillslope scale. *Hydrology and Earth System Sciences*, *21*(11), 5891–5910. https://doi.org/10.5194/hess-21-5891-2017

Vereecken, H., Huisman, J. A., Bogena, H., Vanderborght, J., Vrugt, J. A., & Hopmans, J. W. (2008). On the value of soil moisture measurements in vadose zone hydrology: A review. *Water Resources Research*, *44*(4). https://doi.org/10.1029/2008wr006829

Wagner, H. M. (1969). *Principles of operations research: With applications to Managerial decisions*. Prentice-Hall.

Welch, C., Smith, A. A., & Stadnyk, T. A. (2018). Linking physiography and evaporation using the isotopic composition of river water in 16 Canadian boreal catchments. *Hydrological Processes*, *32*(2), 170–184. https://doi.org/10.1002/hyp.11396

Wurster, P. M., Maneta, M., Kimball, J. S., Endsley, K. A., & Begueria, S. (2020). Monitoring crop status in the continental United States using the SMAP level-4 carbon product. *Front Big Data*, *3*, 597720.